

## Response to Reviewer #1

We thank the reviewer for the helpful comments on the manuscript. Our point-to-point responses to each comment are as follows (reviewer comments are in black, and author responses are in blue).

### I. General Comments

I recommend for this manuscript to be published in Atmospheric Measurement Techniques after revision. The manuscript is a significant contribution to the atmospheric TOF-CIMS literature providing a new method for generating a broad suite of reagent ions via electrospray. The elimination of radioactive ion sources is of great importance as these instruments are routinely deployed throughout the world. Moreover, the authors do a good job implementing the full suite of available procedures for characterizing the novel chemical ionization source (flow rate considerations, calibration with authentic standards, determination of backgrounds and LODs, high-resolution analysis of a complex mixture, voltage scanning, and multiple reagent ion comparisons). I would also like to applaud the authors for acknowledging that this is a work in progress; off-axis spray configurations, sheath gas flow, the positioning of the emitter to tune the reaction time, curtain gas (or counter)  $N_2$  gas flow are all standard features on modern ESI-MS instruments and should improve this system's performance, but these considerations are outside the scope of prototype design and proof of concept experiments.

My only general concern with this manuscript is with the introduction. The authors provide good context for why this work is important and where it fits within the development TOF-CIMS methods and applications. It has, however, been known since 1986 that the electrospray of pure solvents are capable of ionizing gas phase species (see C.M. Whitehouse, F. Levin, C.K. Meng, J.B. Fenn, Proceedings of the 34th ASMS Conference on Mass Spectrometry and Allied Topics). This technique was formalized by Herbert Hill's group and termed secondary electrospray ionization (SESI) in 2000. Arguably, the authors have better controlled the chemistry of this ion source by isolating the electrospray plume from the incoming sample making this truly a chemical ionization source and not SESI. Even this claim is not entirely clear as the mechanism of SESI has been studied for years and no clear conclusion has been reached as to whether SESI ionization proceeds via interaction with small droplets, gas phase ions or other phenomenon. With this being the case, the extensive literature and the diversity of instrumental configurations utilizing electrosprays for the detection of gas-phase species and vapors necessitates placing this work in the broader context of the field. I highly encourage the authors to revisit the broader mass spectrometry literature and at a minimum comment on past work with electrospray plumes for detecting gas-phase species.

I have split my specific comments section into two parts: Major Specific Comments and Minor Specific Comments. There are claims in this manuscript that lack evidence, but I think some of these concerns are addressable with available data. My hope is that these Major Specific

Comments will only lead to a more convincing publication as the claims about ELVOC dimers have been highly contentious to some critics.

Response: Thanks for your overall positive evaluation of our manuscript and your suggestion on commenting past work with secondary electrospray ionization (SESI) technique for detecting gas-phase species. We have added the following paragraph to the introduction.

“It has been known since 1986 that the electrospray plumes cannot only ionize solvated analytes, but also are capable of ionizing gas phase species (Whitehouse et al., 1986; Chen et al., 1994). The later technique was termed secondary electrospray ionization (SESI) (Wu et al., 2000; Tam and Hill, 2004). SESI-MS has been demonstrated promise in the real-time analysis of a variety of gas phase analytes, including drugs (Wu et al., 2000; Meier et al., 2012), explosives (Tam and Hill et al., 2004; Aernecke et al., 2015), human metabolites (Martínez-Lozano et al., 2011; García-Gómez et al., 2015), electronic cigarette vapors (García-Gómez et al., 2016), as well as volatile emissions from bacteria cultures (Zhu et al., 2010), food (Bean et al., 2015; Farrell et al., 2017), and plants (Barrios-Collado et al., 2016). In SESI, the electrospray plume and incoming sample flow intersect in the ionization region, and analyte ionization proceeds likely via interactions with both small charged droplets and electrospray-produced gas phase reagent ions (Wu et al., 2000). In the present study, by coupling the electrospray source to an orthogonal continuous-flow atmospheric pressure IMR region via an evaporation region, we separate the electrospray plume from the incoming samples to avoid SESI, and instead allow for gas-phase chemical ionization.”

## II. Major Specific Comments

1. Lines 337-339: This is not an entirely correct interpretation of clustering and high-resolution peak fitting in the HR-TOF-CIMS. It is absolutely possible to determine whether ions observed using acetate CIMS are ion-neutral clusters or individual ions via voltage scanning techniques and/or a properly configuring the instrument. This is clearly shown in Brophy and Farmer, 2016, which the authors cite in this section. The HR-TOF-CIMS can be operated such that the probability of observing clusters is ridiculously small, but as Brophy and Farmer point out, operation in this mode may cause fragmentation of high molecular weight ELVOC-like molecules.

At sufficiently high  $m/Q$ , the ability to unambiguously distinguish iodide containing clusters from either non-iodide containing ion-neutral clusters and individual ions also becomes potentially nebulous. While the large negative mass defect of iodide certainly aids high-resolution analysis, it is not a panacea for high-resolution molecular formula assignment and the identification of clusters.

This manuscript deals with many other reagent ions that undergo clustering (meaning the instrument is operated in a cluster-transmitting mode), it would also be worthwhile to discuss the

limitations and advantages of  $\text{Li}^+$ ,  $\text{Na}^+$ ,  $\text{K}^+$ , and  $\text{NH}_4^+$  for high-resolution analysis. I would imagine that confident assignment of high-resolution ions would be as problematic for this set of positive ion as running acetate in a cluster-transmitting mode with no voltage scanning experiments.

Response: We agree with the reviewer that voltage scanning techniques and/or a proper instrument configuration may enable distinguishing between the ion-neutral clusters and the individual ions in the acetate mode, and that confident assignment of ions in the iodide mode may become difficult at sufficiently high  $m/Q$ . High resolution analysis showed that the vast majority of ions in  $\text{Li}^+$ ,  $\text{Na}^+$ ,  $\text{K}^+$ ,  $\text{NH}_4^+$ , and  $\text{NO}_3^-$  modes could be assigned to the respective reagent ion-neutral clusters with reasonable molecular formulae based on the minimal mass error criteria and with a spectral pattern very similar to that of Iodide clusters. The unique  $m/Q$  and in some cases presence of nitrogen helped identify the cluster composition. While our focus did not include organic nitrates, we would suggest using  $^{14}\text{N}$  labeled  $\text{NH}_4^+$  or  $\text{NO}_3^-$  in such cases.

In the revised manuscript, we have modified the statements in lines 334-339 (changes underlined):

“The iodide clusters can be easily distinguished from iodide-free molecular ions due to the large negative mass defects of iodide (Lee et al., 2014), although this advantage weakens at sufficiently high masses ( $> \sim 500 m/Q$  for a resolution of 5000). In contrast, broadly distinguishing between acetate-neutral clusters and individual ions in the acetate mode remains a challenge when using non-isotopically labeled acetate as the reagent ion and operating the instrument in a cluster-transmitting mode with no comprehensive voltage scanning experiments (Lopez-Hilfiker et al., 2015; Brophy and Farmer, 2016), as is the case in the present study. As a result, the high-resolution ions observed in the acetate mode cannot be confidently assigned to  $\alpha$ -pinene ozonolysis products and are excluded from further discussions.”

2. Lines 423-430: Brophy and Farmer 2016 performed voltage scanning experiments using multiple adjacent components throughout the atmospheric pressure interface. If clusters are being formed in the first or second quadrupole regions (or during the transitions from one stage to another), then it would not have been possible to eliminate the presence of acetate clusters using adjacent components in the first quadrupole. Additionally, the reagent ion-clusters are most likely ejected from a stable trajectory after an energetic collision. This makes it very unlikely that the reagent ion will 1) re-combine with a neutral species, 2) find its way back into the ion beam or remain in the ion beam and 3) be transmitted through the second segmented quadrupole with a stable enough trajectory to make it to the last portions of the atmospheric pressure interface. This argument as to why a signal increase occurs as the voltage difference is initially increased is highly unlikely if not completely incorrect. The argument presented in lines 422-423 is simple and makes much more sense: ion transmission efficiency in positive mode simply increases a bit with a slight increase in voltage difference for this specific set of components. Slight increases in

voltage difference should drive ions into the second quadrupole more efficiently, and since these ion-neutral clusters are quite stable, the increased kinetic energy basically doesn't matter. The observation would probably be different for very weakly bound clusters.

Response: We have not done detailed ion trajectory modeling of ions and neutral collisions within the quadrupole ion guides and so we cannot comment on the reviewers' suggestion, though it is certainly a reasonable hypothesis. We have tempered our conclusion regarding secondary ion chemistry in the ion guides, and instead combined it directly with the explanation of potential changes in mass transmission.

We have deleted the discussions in lines 422-429 and added the following statement to the revised manuscript.

“The reason for the initial increase in cluster signals is unclear, but might involve secondary ion chemistry and/or slight changes in ion transmission efficiency of the instrument.”

3. Lines 434-444: “...the cluster signals for smaller dimers generally decay more slowly than those for large dimers, suggesting these positive ions can more strongly bind to the smaller dimers, likely due to the higher polarity or the smaller steric effect for smaller dimers... This behavior implies these dimers are most likely covalently-bound species... rather than noncovalently-bound species formed during alpha-pinene ozonolysis”

The fact that smaller dimers decay more slowly than large dimers could also be explained with the alternative hypothesis that two smaller monomers (or one monomer and another small oxidation product) are clustered to the reagent ion. In this scenario, the smaller neutrals would also be more strongly bound to the reagent ion for the exact same reasons (less steric effects and higher polarity) than the larger monomers (or other oxidation products) clustered as a 3-body cluster.

This argument can be made more convincingly by showing the monomer declustering scans. Does this same trend hold true for the C-8 through C-10 monomers (which are most like the >C-10 dimers)? Does this same behavior hold true for dimers detected with nitrate CI and iodide CI?

The authors may already have the data to further understand the behavior of single vs multiple neutral-ion clusters. They note earlier in the manuscript (line 349) that they observe  $\text{NO}_3(\text{NaNO}_3)_n^-$ . While this is substantially different from ELVOC/HOM type hydrocarbons, this does present an interesting example of 3-body and higher-order clusters. What do the voltage scans of these clusters look like? What is the dV50 as a function of the number of  $\text{NaNO}_3$  neutrals? Should we expect 3-body clusters consisting of two neutrals to be more or less stable than 2-body ion-neutral clusters?

This is a contentious area of HR-TOF-CIMS and nucleation/cluster chemistry. This is not “direct” evidence that these potential-dimers are strongly bound as we don’t really know they are, in fact, covalently bonded molecules given the data presented.

I recommend either substantially reworking this section or providing additional evidence via the largest monomers,  $\text{NO}_3(\text{NaNO}_3)_n^-$  clusters, and behavior of the dimers in iodide and nitrate experiments. Given the amount of additional data I am suggesting here, it may be better to actually remove this claim from this paper as it is outside the scope of characterizing and showing the promise of ESCI. This could be an impactful standalone paper if the additional data are consistent. Further study is likely warranted.

Response: We cannot rule out the possibility that two smaller monomers are strongly bound to the reagent ions forming non-covalently bound dimers based on the data presented in the manuscript. We have rephrased the conclusion that these dimer ions have a binding energy approaching that of a covalent bond. A  $\Delta V_{50}$  of  $\sim 15\text{V}$  is a binding enthalpy of  $\sim 80\text{ kcal/mol}$  according to Figure 4 of Lopez-Hilfiker et al., AMT, 2016. Additional data on declustering scans of monomers,  $\text{NO}_3(\text{NaNO}_3)_n^-$  clusters, and dimers in iodide and nitrate modes may help further understand the behavior of ion-neutral clusters and the formation mechanism of dimers. However, as the reviewer pointed out, this is out of the main scope of the present study. Therefore, as suggested by the reviewer, we have removed the discussion on the dimers presented in lines 437-444.

### III. Minor Specific Comments

1. Lines 126-128: Here the author’s present “preliminary fluid dynamic simulations” that suggest the flow rates in which the flow profiles remain laminar. Previous work with the Aerodyne/Tofwerk HR-TOF-CIMS have evaluated this problem in the IMR by simply introducing a calibration gas flow until a stable signal is reached. Then, the calibration gas is shut off and the decay monitored to determine an e-folding time (or similar metric). This is an easy and direct method for understanding the mixing of gases in these reactors. If this source improves the e-folding time over the conventional Aerodyne/Tofwerk IMR design, this ion source could be quite an improvement!

Response: We have determined the e-folding time of ESCI source/atmospheric pressure orthogonal IMR design using nitric acid standard gas in the iodide mode. Figure R1 shows the changes in ion signal for  $\text{I}(\text{HNO}_3)^-$  upon adding or shutting off the standard gas at an ion source flow of 1 slpm and sample flow of 5 or 10 slpm. The increase and decay of ion signal give an e-folding time of about 1s for nitric acid under two different flow conditions. This time response value is comparable to or better than that for the low pressure IMR (1 second to a few seconds).

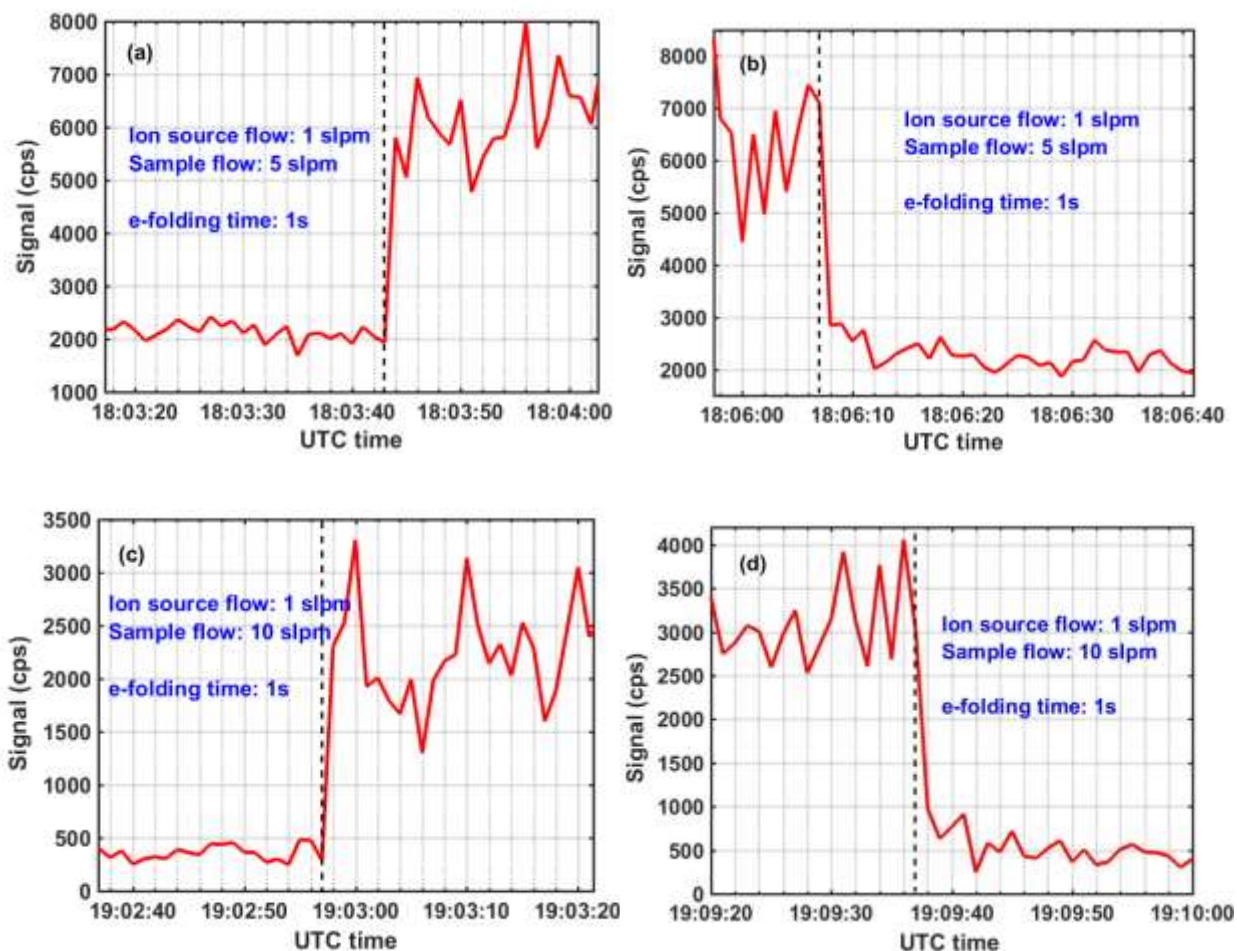


Figure R1 Time series of  $I(\text{HNO}_3)^-$  observed when sampling (a, b) 5 slpm or (c, d) 10 slpm humid room air containing  $\text{HNO}_3$  gas. The ion source flow was 1 slpm. The dashed line indicates the time at which the standard gas was added or shut off.

We have added Figure R1 and following paragraph to the revised manuscript.

“The time response of ESCI source/atmospheric pressure orthogonal IMR design was determined using nitric acid standard in the iodide mode.  $\text{HNO}_3$  was delivered from a permeation tube using a small ( $< 100$  sccm) continuous flow UHP  $\text{N}_2$  through a 3 mm OD Teflon tube to the inlet of the orthogonal IMR. Figure 4 shows the changes in ion signal for  $I(\text{HNO}_3)^-$  upon placing the  $\text{HNO}_3$  delivery line at the opening of a 10 cm length of 2.5 cm OD Teflon tubing serving as the inlet to the IMR or removing the delivery line away from the inlet. Tests were conducted at an ion source flow of 1 slpm and sample flow of 5 or 10 slpm. The increase and decay of  $I(\text{HNO}_3)^-$  signal relative to that from  $\text{HNO}_3$  in the laboratory air give an e-folding time of about 1s for nitric acid under two different flow conditions. This time response value is comparable to or better than that for the low pressure IMR (1 second to a few seconds).”

2. Lines 138-146: This section could use some clarification as to how the electrospray solvent is being pushed through the electrospray emitter. Conventional electrospray configurations use syringe pumps or HPLC/UPLC style solvent pumps with online feedback control making the use of a pressure driven solvent flow a bit different. This could, perhaps, be addressed in Figure 1 by showing the pressure controller, electrospray liquid reservoir, and high voltage connections. Additionally, have the authors measured the solvent flow rate? This is commonly used to distinguish between nano-ESI and standard ESI sources.

Response: To clarify how the electrospray solvent is driven through the electrospray emitter and how the voltage is applied to the electrospray solvent, we have added the pressure controller, electrospray liquid reservoir, and high voltage connections to the schematic of ESCI module (see Figure R2). In addition, we have modified the descriptions in lines 138-141 (changes underlined).

“During operation, a dilute salt solution (~0.05 wt%) in HPLC-grade methanol (MEOH) is biased at the reservoir to +/- (2-5) kV depending on the ion mode by connecting a stainless steel rod immersed into the solution to a high voltage power supply. The solution reservoir is maintained at approximately 50 mbar above atmosphere using a commercial pressure controller (FLUIGENT, model MFCS-EZ) with 0.05 mbar precision. As a result, the salt solution is pushed through the fumed silica capillary tube to the spray needle by the pressure in the reservoir bottle.”

We have not measured the solvent flow rate through the spray needle, but based on macroscopic volume changes in the reservoir, the flow rates are likely less than 100 nL/min.

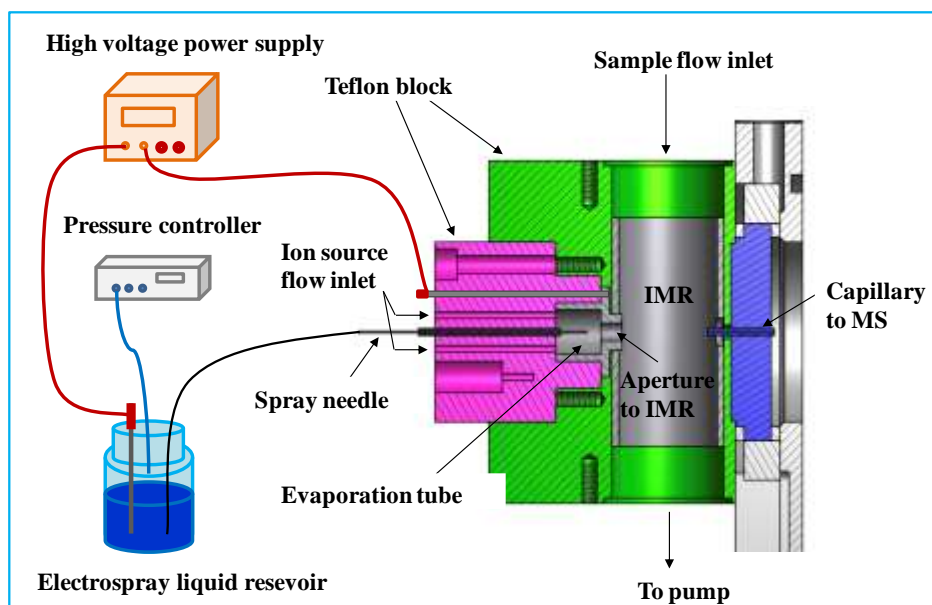


Figure R2 Schematic of the electrospray chemical ionization (ESCI) source module

3. Lines 138-146: I am also curious why the electrospray voltage to reagent ion signal relationship was not investigated? The electrospray voltage is typically a key parameter and is

more complex in this source; the authors point this out by addressing that the ion drift/reaction time depends on the voltage difference between the emitter and the inlet capillary.

Response: We regret leaving this information out. We have investigated the effect of the electrospray voltage on reagent ion signals by varying the reservoir solution voltage ( $V_R$ ) from +/- (2-5) kV. At a given  $V_R$ , the voltage applied to the evaporation tube and IMR ( $V_L$ ) was carefully tuned to get the best ion signals ( $S_{max}$ ), as well as the corresponding  $V_L$ , i.e.,  $V_L(S_{max})$ . In the  $V_R$  range of 2-5 kV, a larger  $V_R$  (with a larger  $V_L(S_{max})$ ) gives a higher reagent ion signal. In general, we found a fairly smooth curve above a threshold voltage for the reservoir, below which the spray was not stable. We found optimal performance with  $V_R$  values of 5 kV (corresponding  $V_L(S_{max}) = 2.8$  kV) and -5 kV (corresponding  $V_L(S_{max}) = -3.5$  kV) for positive ion and negative modes, respectively. We did not probe  $V_R$  values higher than 5 kV due to limitations of various power supplies available.

We have modified the sentences in lines 138-139 (changes underlined):

“During operation, a dilute salt solution (~0.05 wt%) in HPLC-grade methanol (MEOH) is biased at the reservoir to +/- (2-5) kV depending on the ion mode by connecting a stainless steel rod immersed into the solution to a high voltage power supply. At a given reservoir solution voltage ( $V_R$ ), the voltage applied to the evaporation tube and IMR ( $V_L$ ) was carefully tuned to get the best ion signals ( $S_{max}$ ), as well as the corresponding  $V_L$ , referred to as  $V_L(S_{max})$ . In the  $V_R$  range of 2-5 kV, a larger  $V_s$  (with a larger  $V_L(S_{max})$ ) gives a higher reagent ion signal. In order to obtain good ion signals, for most of the measurements performed in this study,  $V_R$  values of 5 kV (corresponding  $V_L(S_{max}) = 2.8$  kV) and -5 kV (corresponding  $V_L(S_{max}) = -3.5$  kV) were used in the positive ion and negative ion modes, respectively.”

4. Lines 165-170: The use of methanol and salts is an interesting choice of reagent ion precursors. Have the authors considered the possibility or looked for any evidence of methanol/protonated-methanol clustering? Additionally, other solvents could be used such as acetonitrile, which typically exhibits less clustering effects in standard electrospray ion sources.

Response: We did not see evidence of protonated methanol clustering in the positive mode, but did see iodide-methanol clustering in the iodide mode when the voltage difference between the first and second quadrupoles is small ( $\Delta V < 2V$ ). However, under typical operating conditions in the present study ( $\Delta V = 4$ ), the iodide-methanol cluster signals became negligible due to declustering.

We have added following sentences after line 170.

“No evidence of protonated methanol clustering was observed when electrospraying a methanolic solution of the described salts except at the extreme voltage differences between the lens and entrance capillary where it was likely a discharge developed. Although the reagent ion

is likely solvated by methanol initially, the sensitivity of the ionization to various trace gases did not appear to be significantly affected in the present study.”

We have not tried acetonitrile, but will certainly consider it in the further development and characterization of the ESCI source.

5. Lines 268-273: Here the authors address the differences in calibrations between atmospheric pressure ESCIMS and low-pressure CIMS. They attribute the differences to ion source configuration, pressure and ion-optics voltage settings. Tofwerk’s Thuner voltage optimization tool would be a great way to ensure that the voltage configurations are optimized across sources. This also appears later in the manuscript where the authors comment on the differences between positive and negative ion modes.

Response: We agree. The present study focuses on the characterization and performance assessment of the ESCI source. The voltage configurations within the vacuum chamber of the instrument were not optimized in this work, and voltage optimization will be considered for the further characterization and application of the ESCI source.

6. Line 328-329: why was the 5 cps criteria chosen for the high-resolution fitting cutoff? Does this correspond to some significant signal-to-noise ratio? Eyeball test? Some justification of this number is required as various other recommendations have been suggested in the HR-TOF-CIMS literature for what constitutes a significant signal.

Response: This cutoff was somewhat ad hoc, and not based on a rigorous signal to noise criterion as we were interested in comparing several different spectra in a broad sense. As we argued in the manuscript, many of these ions might be of importance to various mechanisms of particle growth or organic radical chemistry, but identifying the composition of every ion in these spectra is beyond the scope of this paper.

To clarify why 5 cps criteria was chosen for the high-resolution fitting cutoff, we have modified sentences in lines 327-331 (changes underlined):

“High resolution peak fitting was performed and reasonable molecular formulae were assigned for detected ions that have intensity higher than 5 cps in all seven ion modes. Many ions are present at < 5 cps, which were excluded from the high-resolution fittings to ease the number of identifications required for comparison of several different spectra. Although these lower signal ions might be of importance to various mechanisms of particle growth or organic radical chemistry, identifying their compositions was deemed beyond the scope of this paper.”

7. Lines 348-350: The presence of  $\text{I}(\text{NaI})^-$  and  $\text{NO}_3(\text{NaNO}_3)_n^-$  suggests that the reagent ions generated from this ESCI source are not identical to the reagent ions generated from

conventional Po-210 based methods. This may explain why the mass spectrum obtained for alpha-pinene ozonolysis are similar but not identical to Lopez-Hilfiker et al., 2015 results.

Response: The difference in the composition of reagent ions generated by ESCI and Po-210 sources may help explain why the mass spectra obtained for  $\alpha$ -pinene ozonolysis are not identical in the two studies. However, different voltage settings and instrument configurations in the two studies can also lead to differences in the mass spectra. Iodide adducts are likely weaker than most of the other adducts studied, and thus most sensitive to instrumental parameters.

8. Lines 368-371: It might be worth adding a figure to better illustrate the difference between these various reagent ions. For example, a histogram of O:C or oxidation state by high-resolution assignment could help to highlight these differences. This provides a great opportunity to further show that reagent ions are compound-class specific and parallels the previous work of Aljawhary et al., 2013. I think that bulk metrics (i.e. average oxygen:carbon ratio) would be less informative.

Response: We have added a figure showing boxplots with 5 different percentiles for the O:C ratio of monomeric products from  $\alpha$ -pinene ozonolysis detected in  $I^-$ ,  $NO_3^-$ , and  $Na^+$  modes (See Figure R3). We have also added the following paragraph to the revised manuscript.

“Figure 11 shows boxplots for the O:C ratio of monomeric products from  $\alpha$ -pinene ozonolysis detected in  $I^-$ ,  $NO_3^-$ , and  $Na^+$  modes. The O:C values for all the percentiles observed in  $I^-$  and  $NO_3^-$  modes are overall similar, whereas the corresponding values observed in  $Na^+$  mode are obviously smaller. In addition, more than half of products observed in the three modes have a O:C ratio larger than 0.8. These results are consistent with the observations from Figure 10, where  $I^-$ ,  $NO_3^-$ , and  $Na^+$  are all sensitive to highly oxygenated organics, but the former two reagent ions are insensitive to less oxygenated organics as compared to  $Na^+$ .”

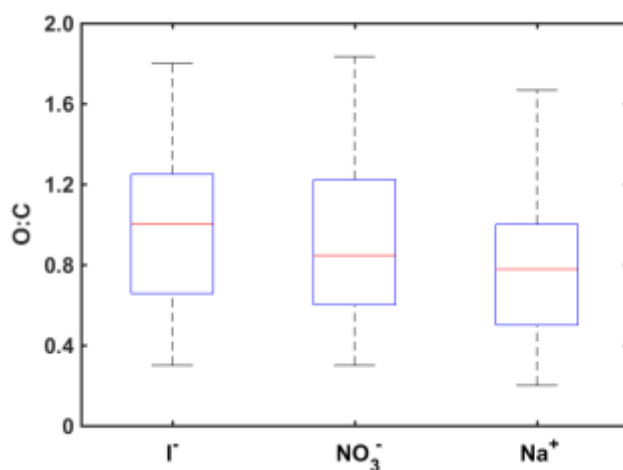


Figure R3 Boxplots showing the 5th, 25th, 50th, 75th, and 95th percentiles for the O:C ratio of monomeric products from  $\alpha$ -pinene ozonolysis detected in different ion modes.

#### IV. Technical Corrections

1. Line 85: remove double “..”

Response: We have revised it.

2. Line 116: please specify the manufacturer/model if this is a commercial silica spray needle or simply a piece of fused silica tubing

Response: We have specified the manufacturer/model of the silica spray needle and fused silica tubing.

3. Line 126: what type of pump was used to back the IMR? Was the flow controlled via mass flow controller or some other device?

Response: The IMR was backed by a dry scroll vacuum pump (IDP-3, Agilent Technologies) and the flow was controlled by a mass flow controller. We have stated this in the revised manuscript.

4. Line 139: the electrospray solvent reservoir is biased between 3-5 kV. Should this read something like “+/- 3-5 kV depending on the ion mode”? Typical electrospray systems require different voltage magnitudes depending on the ion mode (positive vs negative) with negative mode typically requiring higher negative potentials. This would be useful information.

Response: We have changed “...biased at the reservoir to 3-5 kV” to “...biased at the reservoir to +/- (3-5) kV depending on the ion mode”.

For both positive and negative ion modes, voltages magnitudes applied to the electrospray solvent reservoir ( $V_R$ ) are the same, but the voltages applied to the evaporation tube and IMR ( $V_L$ ) are different. For example, when  $V_S = +/- 5$  kV,  $V_L$  for the best ion signals is 2.8 kV in the positive ion mode and -3.9 kV in the negative ion mode (see the reply to Minor Specific Comments #3).

5. Similar to item 2 in the specific comments section: It would be useful to show the electrospray solvent reservoir, pressure controller, and HV connections in Figure 1 as the experimental configuration is not totally clear.

Response: We have added electrospray solvent reservoir, pressure controller, and HV connection components to the schematic of the ESCI module (see Figure R2).

6. Figure 2a appears to have error bars while figure 2b does not.

Response: Figure 2b shows the dependence of the ion signal on the sample flow with an ion source flow/sample flow ratio of 0.1. We did not repeat the experiments for the same conditions,

but instead we did the same measurement at ion source flow/sample flow ratios ranging from 0.02-0.2. The trend of the ion signal vs. the sample flow at each flow ratio is very similar to that shown in Figure 2b, though the absolute ion signal values are different.

7. Figure 3's caption reads "normalized sensitivity" while the y-axis reads signal in counts per second. Should the units be normalized counts per second (ncps) and/or "normalized signal"?

Response: We have changed y-axis label in Figure 3 to "normalized signal".

## Response to Reviewer #2

We thank the reviewer for the helpful comments on the manuscript. Our point-to-point responses to each comment are as follows (reviewer comments are in black, and author responses are in blue).

The authors describe a characterization study on a new ion source which is tailored for field-deployable time-of-flight mass spectrometers, which are widely used by the atmospheric science community. The procedure of electrospraying methanolic salt solutions of alkali metals and ammonium for positive ion generation is described as a major advantage compared to radioactive source materials, which are subject to certain restrictions and regulations. Gas-phase measurements are demonstrated for a limited number (three) of standards, and ion-source flow and humidity dependencies are investigated. The application of the source with four different cluster ion systems ( $\text{Li}^+$ ,  $\text{Na}^+$ ,  $\text{K}^+$  and  $\text{NH}_4^+$ ) is demonstrated using  $\alpha$ -pinene ozonolysis as a surrogate system for ambient SOA.

While the manuscript certainly falls into the scope of AMT, I have some major objections that need to be addressed before publication.

1) The manuscript does not provide a sound argument why the presented technique is an alternative to already existing techniques, such as e.g. proton-transfer reaction (PTR) technology. While the argument of providing a non-radioactive way of charge generation is certainly valid, the authors only indirectly mention (by the citation of e.g. Veres 2008 and Yuan 2016) that a common way to generate ions for atmospheric measurements is the use of hollow cathodes or corona discharge.

A certainly novel characteristic of the described technique is the sampling with an orthogonal high flow rate at atmospheric pressure across the inlet capillary, which likely reduces sampling losses of highly oxidized, low-volatile compounds. The presented design enables the authors to measure oxidized monomers and dimers of  $\alpha$ -pinene oxidation in the gas phase that are usually not accessible with common PTR inlets. However, Breitenlechner et al. (2017) recently have shown that PTR ionization using charged water clusters as reagent ions is sensitive towards monomeric and dimeric  $\alpha$ -pinene oxidation products in the gas phase at ppqv levels. This demonstrates that the gas inlet design is crucial for successfully measuring highly oxidized compounds in the gas phase. Breitenlechner et al. demonstrated that the whole volatility spectrum of VOCs, SVOCs, LVOCs and ELVOCs can be covered by PTR and thus it is questionable that one needs multiple complementary ionization schemes (as stated in l. 80).

Response: We appreciate the reviewer's point, and have added a reference to the new PTR-3 to the introduction as it is showing an impressive sensitivity to a wide range of organic compounds. Our experience has been that each reagent ion chemistry has advantages and disadvantages depending upon the analytical goal. Adduct ionization can lead to humidity dependencies or ion-

induced dimers (as discussed herein), while reactive charge transfer methods such as PTR can lead to water loss from alcohols or nitric acid loss from nitrates and thus changes in the spectrum compared to the sample as discussed in Blake et al. (2009).

One of the major characteristic of the CIMS techniques including PTR technology is their high selectivity. The volatility and polarity spectra of the targeted species largely depend on the selection of reagent ions. Although a specific reagent ion may sensitively detect species spanning a wide spectrum of volatility or polarity, it may not be able to cover all of the species presented within the spectrum. For example, as presented in this study, the  $\text{Na}^+$  reagent ion is sensitive to the species covering the volatility spectrum of VOCs, SVOCs, LVOCs, and ELVOCs, as well as the polarity spectrum of less oxygenated and highly oxygenated species. However, some species such as the very small species ( $\text{CH}_2\text{O}_2$ ,  $\text{CH}_2\text{O}_3$ , and  $\text{C}_2\text{H}_2\text{O}_3$ ) and certain highly oxygenated species detected by  $\text{I}^-$  and  $\text{NO}_3^-$  are not detected or sensitively detected by  $\text{Na}^+$ , presumably because of the low sensitivity to these specific species.

Moreover, this comment seems only relevant to organic compounds, but there is continued interest in a suite of inorganic vapors for atmospheric chemistry including halogens, reactive nitrogen oxides, and reduced nitrogen species which may be detected well by some ionization methods and not others. Therefore, multiple complementary ionization schemes are needed to obtain a comprehensive view of a complex chemical system such as that found in the atmosphere.

The electrospray chemical ionization (ESCI) source presented in this work provides an alternative to radioactive sources and allows the production of reagent ions (e.g.,  $\text{Li}^+$ ,  $\text{Na}^+$ ,  $\text{K}^+$  and  $\text{NH}_4^+$ ) that are largely unavailable in current CIMS techniques, including ionization methods that utilize hollow cathodes or corona discharge methods. Thus, the work provides a new alternative form of ionization with a good deal of flexibility to study ionization of compounds by adduct formation across a range of binding enthalpies.

2) The authors state that the main advantage of CIMS is the inherently quantitative character when applying the kinetic theory of gases. To estimate the upper limit ionization efficiency it is a prerequisite that the flows in the IMR region are laminar in order to calculate the interaction time between ions and neutrals. Any flow disturbance or pressure fluctuation in the ionization region can result in turbulent mixing in which secondary ion interactions can become dominant. Therefore the authors evaluated the design with CFD simulations (not shown) and found that under the investigated conditions flows are in the laminar regime.

However, when using electrospray as a source and sampling ambient air of different humidity, ions do appear solvated by alcohol or water clusters (e.g. Horning, 1974; Garvey, 1994). This implies that the ion mobility of the charged clusters in the IMR is different from the values stated for unsolvated  $\text{NO}_3^-$  and  $\text{Na}^+$  stated in line 145 and thus the interaction time between ion clusters and gas phase analytes is unknown. The fact that water vapour concentration changes the cluster

size distribution (ion source residence time) and thus affects the sensitivity should be added to the discussion in l. 274 ff.

Furthermore, it can also not be excluded that secondary reactions occur in the ion transfer optics hindering the estimation of ionization efficiency.

Response: We agree that the reagent ions can be solvated by methanol or water clusters in the IMR. Because of the lack of information on the ion mobility of the solvated reagent ions, the reaction time between these reagent ions and gas phase analytes in the IMR is currently unknown. However, given that the ion mobility of solvated ions is generally smaller than unsolvated reagent ions, the actual ion-molecule interaction time in the IMR is expected to be longer than that estimated for the unsolvated ions.

We have modified the statement around line 145 (changes underlined):

“Under laminar flow conditions, the reaction time between reagent ions and sampled trace gases in the IMR is mainly determined by the electric field-induced drift velocity of the reagent ions. For instance, for two reagent ions used in this study,  $\text{NO}_3^-$  and  $\text{Na}^+$ , the ion molecule reaction time (i.e., ion drift time) in the IMR is estimated to be 0.5-1 ms and 0.4-0.7 ms, respectively, with an ion mobility of  $2.37 \text{ cm}^2 \text{ s}^{-1} \text{ V}^{-1}$  for  $\text{NO}_3^-$  (Ellis et al., 1978) and  $3.4 \text{ cm}^2 \text{ s}^{-1} \text{ V}^{-1}$  for  $\text{Na}^+$  (Bohringer et al., 1987) under typical operation conditions (2-4 kV across the IMR). However, when using electrospray as a source and sampling ambient air of different humidity, the reagent ions can be solvated by methanol or water clusters (Horning et al., 1974; Garvey et al., 1994). As the ion mobility of solvated reagent ions is likely smaller than the values for unsolvated reagent ions, the ion-molecule reaction time between solvated reagent ions and gas phase analytes in the IMR is expected to be longer than that estimated for the unsolvated ions.”

We have also modified the paragraph in lines 274-281 (changes underlined):

“The presence of water vapor can affect sensitivities, either by competing for  $\text{I}^-$  ions, thus lowering the sensitivity, or by accommodating excess energy from the collision to stabilize the Iodide-molecule clusters, thereby increasing the sensitivity (Lee et al., 2014; Iyer et al., 2016). Water vapor may also affect sensitivities by changing the size distribution of reagent ion clusters and thus their residence time (ion-molecule reaction time) in the IMR. Moreover, water vapor can affect the transmission of soluble gases through sample tubing. It is difficult to evaluate the effect of changing cluster size distribution as the information regarding the distribution and ion mobility of the reagent ion clusters is currently unavailable. In the current configuration of the ESCIMS, it is also difficult to isolate the sample transfer effect experimentally as done previously in low-pressure IMR regions by using separate delivery lines for calibrants and water vapor. Thus, our results shown here reflect a combination of ionization efficiency, cluster distribution, and sample transfer aspects.”

The secondary reactions in the ion transfer optics cannot be ruled out, but they are usually assumed to be negligible for estimating the maximum sensitivities.

3) The list of reagent ions in CIMS (l. 69) does not mention protonated ethanol for selective measurements of gas phase  $\text{NH}_3$ , DMSO and VOCs (Nowak, 2002). In addition to this, I wonder what would be seen with the described system when using only methanol instead of a methanolic solution of the described salts. In theory methanol has a slightly smaller proton affinity than ethanol (7.9 vs 8.2 eV) and one might observe ionization by proton transfer reactions from methanol electrospray itself (via the reagent ion clusters  $(\text{CH}_3\text{OH})_n\text{H}^+$ ).

Furthermore, are proton transfer reactions observed when using  $\text{NH}_4^+$  as reagent ion?

Response: Thanks for catching this oversight. We have modified the sentence in line 69 (changes underlined):

“The reagent ions used mainly include  $\text{I}^-$ ,  $\text{NO}_3^-$ , acetate,  $\text{CF}_3\text{O}^-$ , and  $\text{SF}_6^-$  for negative ion CIMS, and  $\text{H}_3\text{O}^+$ ,  $\text{NO}^+$ , protonated ethanol, and benzene cation for positive ion CIMS.”

We have not tried using only methanol as the electrospray liquid. However, we did not see evidence of protonated methanol clusters when electrospraying a methanolic solution of the described salts. Our comparisons of spectra also do not provide any obvious evidence for proton transfer reactions when using  $\text{NH}_4^+$  as the reagent ion for the a-pinene ozonolysis system.

We have also added the following statement after line 170:

“No evidence of protonated methanol clustering was observed when electrospraying a methanolic solution of the described salts except at the extreme voltage differences between the lens and entrance capillary where it was likely a discharge developed. Although the reagent ion is likely solvated by methanol initially, the sensitivity of the ionization to various trace gases did not appear to be significantly affected in the present study.”

4) Electrospray ionization has previously been reported in an extraction mode, in which online measurements of aerosols (Gu, 2010) and especially a-pinene SOA (Doezema, 2012; Gallimore, 2013) has successfully been demonstrated. The apparent question related to these publications and the reported application to chamber studies of a-pinene SOA is: How can the authors rule out that the observed signal does not emerge from aerosol particles? This is not discussed in the manuscript but might have fundamental consequences on the interpretation made in chapter 3.4. The figure that needs to be shown is that the gas phase concentration is independent of SOA mass.

Response: In the present study, the ESCI source is coupled to an orthogonal continuous-flow atmospheric pressure IMR region. Under typical sample flow and ion source flow conditions, the mixed flow in the IMR remains laminar, and the sample flow acts to carry the unevaporated

droplets entering the IMR away from the effective ionization region, thus largely isolating the electrospray plume from incoming samples, making the ESCI source a chemical ionization source rather than extractive or secondary electrospray ionization (EESI or SESI).

The evidence of the ESCI source being a chemical ionization source and not EESI or SESI can be provided by monitoring the signal ratio of  $\text{NO}_3^-/\text{I}(\text{HNO}_3)^-$  when sampling gas phase  $\text{HNO}_3$  in the iodide mode. If the direct interaction between electrospray plume and incoming sample flow is important,  $\text{HNO}_3$  dissolved in charged droplets can dissociate forming  $\text{H}^+$  and  $\text{NO}_3^-$ , leading to the generation of  $\text{NO}_3^-$  ions in the negative ion mode. Therefore, a large signal ratio of  $\text{NO}_3^-/\text{I}(\text{HNO}_3)^-$  is expected. Figure R1 shows the signal ratio of  $\text{NO}_3^-/\text{I}(\text{HNO}_3)^-$  as a function of gas phase  $\text{HNO}_3$  concentration under dry and wet conditions observed in the iodide mode. The signal ratios of  $\text{NO}_3^-/\text{I}(\text{HNO}_3)^-$  are significantly smaller than 0.01 at various  $\text{HNO}_3$  concentrations, suggesting the direct interaction of electrospray plume with incoming samples is not important in the ESCI source.

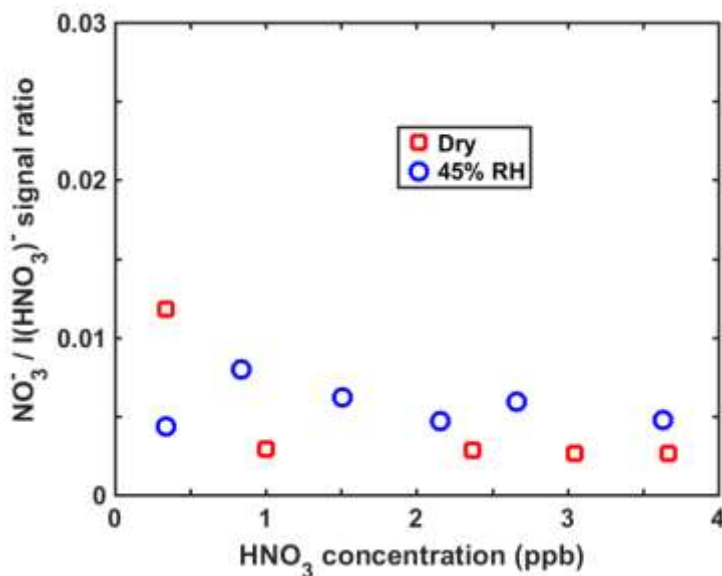


Figure R1 Signal ratio of  $\text{NO}_3^-/\text{I}(\text{HNO}_3)^-$  as a function of  $\text{HNO}_3$  concentration under dry and wet conditions observed using iodide as the reagent ion.

We have added Figure R1 and following paragraph after line 146.

“Under typical operating conditions, the sample flow likely transports any unevaporated droplets away from the effective ionization region in the IMR, thus largely isolating the electrospray plume from the incoming samples, making the ESCI source a chemical ionization source rather than secondary or extractive electrospray ionization (SESI or EESI) source. The evidence of the ESCI source being a chemical ionization source and not SESI or EESI is provided by monitoring the signal ratio of  $\text{NO}_3^-/\text{I}(\text{HNO}_3)^-$  when sampling gas phase  $\text{HNO}_3$  in the iodide mode. If the direct interaction between electrospray plume and incoming sample flow is important,  $\text{HNO}_3$

dissolved in charged droplets can dissociate forming  $H^+$  and  $NO_3^-$ , leading to the generation of  $NO_3^-$  ions in the negative ion mode. Therefore, a large signal ratio of  $NO_3^-/I(HNO_3)^-$  is expected. Figure 3 shows the signal ratio of  $NO_3^-/I(HNO_3)^-$  as a function of gas phase  $HNO_3$  concentration under dry and wet conditions observed in the iodide mode. The signal ratios of  $NO_3^-/I(HNO_3)^-$  are significantly smaller than 0.01 at various  $HNO_3$  concentrations, suggesting the direct interaction of electrospray plume with incoming samples is not important in the ESCI source.”

5) Chapter 3.4.3: While the work by Lopez-Hilfiker et al. (2016) was conducted at IMR pressure 70 Torr, the reported work samples from an atmospheric pressure IMR. Thus, I assume that the pressure in the transfer ion optics reported in this work is significantly higher than in the work by Lopez-Hilfiker et al. (2016). How does the pressure in the transfer quadrupoles affect the declustering?

Response: In the present work, a stainless steel capillary tube (20 mm long, 0.13 mm ID) acts as the atmospheric pressure interface between the IMR and the vacuum chamber of the MS, and effectively drops the pressure from 1 atm in the IMR to about 1.5 Torr in the first quadrupole of the MS. The pressure in the transfer ion optics in the present study is very similar to that in the work by Lopez-Hilfiker et al. (2016). Thus, the declustering results obtained in the two studies can be compared.

We have modified the sentences in lines 131-133 (changes underlined):

“The SS capillary projects 3.5 mm into the IMR and acts as the atmospheric pressure interface between the IMR and the vacuum chamber of a commercial HRToF-MS (Tofwerk AG, Thun, Switzerland), effectively dropping the atmospheric pressure in the IMR to 1.5 Torr in the first quadrupole of the MS.”

6) The conclusion that the observed dimers are covalently bound molecules instead of non-covalently bound clusters cannot be made, since the authors do not show that ion cluster dimers show a different declustering profile in the Li-mode. Furthermore, the fact that gas-phase dimers are covalently bound molecules was already reported by Kirkby et al. (2016), contrary to the statement in l. 438 ff.

Response: See our response to reviewer 1. We have modified the conclusion that the dimer ions have adduct energies with  $Li^+$  that approach covalent bonds. As the behavior and formation mechanism of dimers is out of the scope of characterizing and showing the promise of ESCI source in the present study, we have deleted the discussions about the dimers in lines 436-444.

Minor comments:

l. 88:  $NH_4^+$  is not a metal cation-  $Li^+$  is missing.

Response: We have revised “certain reagent ions such as metal cations (e.g., Na<sup>+</sup>, K<sup>+</sup>, and NH<sub>4</sub><sup>+</sup>)” as “certain reagent ions such as metal cations (e.g., Li<sup>+</sup>, Na<sup>+</sup>, and K<sup>+</sup>) and NH<sub>4</sub><sup>+</sup>”.

l. 92 - 93: Why is it expected that metal cations are less selective toward HOMs? Furthermore, it is not possible to infer carbon oxidation state from the molecular composition. E.g. an hydroperoxide and an alcohol functional group lead to the same carbon oxidation state but different avg. OSC. Also a carbonyl group is a higher carbon oxidation state than a hydroperoxide.

Response: It is more that the metal cations are more sensitive to less oxygenated compounds than are I<sup>-</sup> and NO<sub>3</sub><sup>-</sup>. Compared to I<sup>-</sup> and NO<sub>3</sub><sup>-</sup>, which are significantly more sensitive to highly oxygenated organic compounds than to less oxygenated ones, the metal cations such as Li<sup>+</sup>, Na<sup>+</sup>, and K<sup>+</sup> are less selective because in our system they can sensitively detect both less oxygenated (e.g, compounds containing only carbonyl groups) and highly oxygenated multi-functional organic species. We are now careful to specify that by carbon oxidation state we mean average oxidation state of carbon in the molecule.

To clarify these points, we have modified the sentences in lines 91-96 (changed underlined):

“Compared to I<sup>-</sup>, NO<sub>3</sub><sup>-</sup>, and acetate, which are significantly more sensitive to highly oxygenated organic compounds than less oxygenated ones (Aljawhary et al., 2013; Lee et al., 2014, Hyttinen et al., 2015; Iyer et al., 2016, Berndt et al., 2016), these metal cations are expected to be less selective toward oxygenated organic compounds and can be used to sensitively detect both less oxygenated (e.g, compounds containing only carbonyl groups) and highly oxygenated multi-functional organic species (Gao et al., 2010; Nguyen et al., 2010; Nizkorodov et al., 2011; Laskin et al., 2012; Witkowski and Gierczak, 2013; Zhao et al., 2015; Tu et al., 2016; Zhao et al., 2016; Zhang et al., 2017)”

l. 133: What is the sample flow of the MS?

Response: The sample flow of MS is about 270 sccm. We have added this to the revised manuscript.

l. 143: Na<sup>+</sup> superscript.

Response: We have revised this.

l. 217: What is the driving force of evaporation? Temperature or dilution into a solvent-free sample flow?

Response: The driving force of evaporation includes both the addition of a flow of ultra-high purity N<sub>2</sub> to the evaporate tube and the dilution into a solvent-free sample flow. However, as the sample flow can quickly carry the unevaporated droplets out of the effective ionization region, the

evaporation of these droplets would not be a major contributor to the total ion signal (see the reply to Major Comments # 4).

Although we did not investigate the temperature effect on evaporation, we believe that a higher temperature (e.g., a heated ion source flow) can further improve the evaporation and is worth considering in the further development and characterization of the ESCI source.

l. 246: Why is the ion molecule reaction time in ESCIMS shorter than in low-pressure CIMS?

Response: The ion-molecule reaction time in ESCIMS is determined by the electrical-induced ion drift velocity of the reagent ions. The lower limit is equal to the residence time of unsolvated reagent ions and is, for example, 0.5-1 ms for  $\text{NO}_3^-$  and 0.4-0.7 ms for  $\text{Na}^+$  when there is 2-4 kV across the IMR. In contrast, the ion-molecule reaction time in low-pressure CIMS is determined by the flow conditions in the IMR and is typically 30 to 120 ms (Lopez-Hilfiker et al., 2016; Bertram et al., 2011; Lee et al., 2014).

l. 307: The background signals in Figure 5a are lower than those written.

Response: Thank you for pointing this out. The y-axis in all mass spectrum figures including Figure 5 actually represents the signal density, i.e.,  $d(\text{Signal})/d(m/Q)$ , and the ion signal is equal to the integration of the peak area. We have revised the y-axis label "Signal (cps)" as " $d(\text{Signal})/d(m/Q)$  (cps)" in all the mass spectrum figures.

l. 327: misspelling: reagent

Response: We have revised this.

l. 424: misspelling: reagent

Response: We have revised this.

l. 429: Why are the declustering scans for the monomers not shown?

Response: Scans for the monomers are discussed in the text, but for example purposes, the differences in the behaviors resulting from the reagent ions  $\text{Li}^+$ ,  $\text{Na}^+$ ,  $\text{K}^+$ , and  $\text{NH}_4^+$  were simply cleaner and clearer using the dimers. These ions have more uncertainty regarding their source and structure and thus provide a scientifically more interesting example. As noted above, in the case of  $\text{Li}^+$ , these dimer ions are very strongly bound and would therefore provide a good test case for quantum chemical modeling of the binding energies of a covalent dimer compared to two monomers surrounding the ion. Thus, we wish to highlight the dimer ions here as monomer ion declustering behaviors for Iodide are shown in this study and discussed in detail in Lopez-Hilfiker et al. (2016).

Figure 8: What is the peak-width of the measured signals in y-direction? Some of the dimers have a very large positive mass defect ( $>0.2$  at  $m/z < 300$ ). What is the elemental composition of these signals?

Response: The peak-width at half height is 0.03 at  $m/z$  127 and 0.07 at  $m/z$  381. The dimers with a mass defect  $> 0.2$  and  $m/z < 300$  have low O:C and high H:C ratios. Their molecular formulae include  $C_{15}H_{28-30}O_2$ ,  $C_{16}H_{30-32}O_{2-3}$ ,  $C_{17}H_{28-30}O_{2-4}$ ,  $C_{18}H_{28-32}O_3$ , etc.

1  
2  
3  
4  
5  
6  
7  
8  
9  
10  
11  
12  
13  
14  
15  
16  
17  
18  
19  
20  
21  
22  
23

An electrospray chemical ionization source for real-time measurement of atmospheric organic and inorganic vapors

Yue Zhao,<sup>1</sup> Jeremy Chan,<sup>1,2</sup> Felipe D. Lopez-Hilfiker,<sup>1,3</sup> Emma L. D'Ambro,<sup>1</sup> Jay G. Slowik,<sup>3</sup> Jeff Riffell,<sup>2</sup> and Joel A. Thornton<sup>1</sup>

- 带格式的: 字体颜色: 自动设置
- 带格式的: 上标
- 带格式的: 字体颜色: 自动设置

<sup>1</sup>Department of Atmospheric Sciences, University of Washington, Seattle, WA 98195, USA  
<sup>2</sup>Department of Biology, University of Washington, Seattle, WA 98195, USA  
<sup>3</sup>Laboratory of Atmospheric Chemistry, Paul Scherrer Institute, 5232 Villigen, Switzerland

*Correspondence to:* Joel A. Thornton (thornton@atmos.washington.edu), Felipe D. Lopez-Hilfiker (felipe.lopez@psi.ch)

- 带格式的: 字体颜色: 自动设置
- 带格式的: 字体颜色: 自动设置
- 域代码已更改
- 带格式的: 字体颜色: 自动设置
- 带格式的: 字体颜色: 自动设置
- 域代码已更改
- 带格式的: 字体颜色: 自动设置
- 带格式的: 字体颜色: 自动设置
- 带格式的: 字体颜色: 自动设置

24 Abstract

25 We present an electrospray ion source coupled to an orthogonal continuous-flow atmospheric  
26 pressure chemical ionization region. The source can generate intense and stable currents of  
27 several specific reagent ions using a range of salt solutions prepared in methanol, thereby  
28 providing both an alternative to more common radioactive ion sources and allowing for the  
29 generation of reagent ions that are not available in current chemical ionization mass spectrometry  
30 (CIMS) techniques, such as alkali metal cations. We couple the orthogonal electrospray chemical  
31 ionization (ESCI) source to a high resolution time-of-flight mass spectrometer (HRTof-MS), and  
32 assess instrument performance through calibrations using nitric acid (HNO<sub>3</sub>), formic acid  
33 (HCOOH), and isoprene epoxydiol (*trans*-β-IEPOX) gas standards, and through measurements  
34 of oxidized organic compounds formed from ozonolysis of α-pinene in a continuous-flow  
35 reaction chamber. When using iodide as the reagent ion, the HRTof-ESCIMS prototype has a  
36 sensitivity of 11, 2.4, and 10 cps pptv<sup>-1</sup> per million cps of reagent ions and a detection limit (3σ,  
37 5s averaging) of 4.9, 12.5, and 1.4 pptv to HNO<sub>3</sub>, HCOOH, and IEPOX, respectively. These  
38 values are comparable to those obtained using an Iodide-adduct HRTof-CIMS with a radioactive  
39 ion source and low pressure ion-molecule reaction region. Applications to the α-pinene  
40 ozonolysis system demonstrates that HRTof-ESCIMS can generate multiple reagent ions (e.g, I,  
41 NO<sub>3</sub><sup>-</sup>, acetate, Li<sup>+</sup>, Na<sup>+</sup>, K<sup>+</sup>, and NH<sub>4</sub><sup>+</sup>) having different selectivity to provide a comprehensive  
42 molecular description of a complex organic system.

43

44 1. Introduction

45 The Earth's atmosphere contains thousands of inorganic and organic species that, through  
46 complex free radical and multiphase chemistry, play a vital role in air quality and climate change  
47 (Finlayson-Pitts and Pitts, 2000; Seinfeld and Pandis, 2006; Goldstein and Galbally, 2007).

域代码已更改

48 Characterizing the identity and abundance of many of these species in the atmosphere is essential  
49 for understanding their atmospheric processes and subsequent environmental and climate  
50 impacts. As a result, there is a critical interest in the development and application of the state-of-  
51 art analytical instruments for the analysis of atmospheric composition (Noziere et al., 2015).

域代码已更改

52 As a sensitive, selective, and soft-ionization measurement technique, chemical ionization mass  
53 spectrometry (CIMS) has received significant use in the real-time *in situ* measurement of  
54 atmospheric trace species (Huey et al., 1995; Fortner et al., 2004; Hearn and Smith, 2004; Smith  
55 et al., 2004; Crouse et al., 2006; Huey, 2007; Veres et al., 2008; Kercher et al., 2009; Zhao et al.,  
56 2010). The recent coupling of chemical ionization to high resolution time-of-flight mass  
57 spectrometers (HRToF-MS) enables the simultaneous determination of the abundance and  
58 molecular composition of a wide array of atmospheric inorganic and organic compounds with  
59 fast time response and high sensitivity (Junninen et al., 2010; Bertram et al., 2011; Yatavelli et  
60 al., 2012; Aljawhary et al., 2013; Lee et al., 2014; Lopez-Hilfiker et al., 2014; Brophy and  
61 Farmer, 2015, 2016; Lopez-Hilfiker et al., 2016a; Yuan et al., 2016). The use of HRToF-CIMS  
62 has allowed groundbreaking progress in atmospheric organic chemistry, such as the observation  
63 of highly oxygenated molecules (HOMs) formed by monoterpene oxidation (Ehn et al., 2014;  
64 Jokinen et al., 2015; Berndt et al., 2016; Lee et al., 2016). Very recently, a newly developed  
65 proton-transfer reaction (PTR) time of flight instrument (PTR-3), has enabled sensitive detection  
66 of a wide range of organic compounds including HOMs (Breitenlechner et al., 2017).

域代码已更改

域代码已更改

域代码已更改

67 In CIMS, the analyte molecule reacts with a specific reagent ion via one or more mechanisms,  
68 including ligand switching reaction forming an ion-molecule adduct (Huey et al., 1995; Kercher  
69 et al., 2009; Aljawhary et al., 2013; Lee et al., 2014; Brophy and Farmer, 2015, 2016), proton  
70 addition (abstraction) forming a protonated (deprotonated) ion (Nowak et al., 2002; Veres et al.,  
71 2008; Yatavelli et al., 2012; Aljawhary et al., 2013; Brophy and Farmer, 2015, 2016; Yuan et al.,  
72 2016), or by direct charge transfer forming a molecular ion (Huey et al., 1995; Kim et al., 2016).

域代码已更改

域代码已更改

域代码已更改

73 The reagent ions used mainly include I, NO<sub>3</sub><sup>-</sup>, acetate, CF<sub>3</sub>O<sup>-</sup>, and SF<sub>6</sub><sup>-</sup> for negative ion CIMS,  
74 and H<sub>3</sub>O<sup>+</sup>, NO<sup>+</sup>, protonated ethanol, and benzene cation for positive ion CIMS. Choosing an  
75 appropriate reagent ion is essential for a comprehensive characterization of a specific class of  
76 molecules while having selectivity to avoid unnecessary congestion of the mass spectrum with  
77 unwanted components. For example, previous studies using NO<sub>3</sub><sup>-</sup> CIMS have reported a very  
78 low yield of HOMs from OH oxidation of monoterpene (Jokinen et al., 2015). However, a recent  
79 study using acetate CIMS found a significantly higher HOMs yields from the same system  
80 (Berndt et al., 2016). The reason for this difference is presumably a lower sensitivity of NO<sub>3</sub><sup>-</sup> to  
81 HOMs formed in OH oxidation of monoterpene than that of acetate (Berndt et al., 2016). On the  
82 other hand, many atmospheric organic systems consist of a wide range of organic compounds

带格式的: 字体颜色: 自动设置

域代码已更改

域代码已更改

域代码已更改

83 with different functionality and polarity. Therefore, multiple complementary ionization schemes  
84 are needed to obtain a broad view of these systems (Aljawhary et al., 2013; Praplan et al., 2015).

域代码已更改

85 Some advantages of CIMS are that it is direct, online, reproducible and inherently quantitative in  
86 that the kinetic theory of gases allows a robust upper limit ionization efficiency, and thus  
87 instrument response, to be calculated knowing only the pressure and interaction time of reagent  
88 ions and analyte molecules. However, the need for gas-phase reagent ions limits the suite of  
89 usable reagent ions to those for which a safe and stable gas-phase precursor exists and which  
90 produce the desired reagent ion cleanly at a high yield when ionized. As such, certain reagent  
91 ions such as metal cations (e.g., Li<sup>+</sup>, Na<sup>+</sup>, and K<sup>+</sup>) and NH<sub>4</sub><sup>+</sup> ~~metal cations (e.g., Na<sup>+</sup>, K<sup>+</sup>, and~~  
92 ~~NH<sub>4</sub><sup>+</sup>)~~, which are commonly used for detection of atmospheric organic compounds in off-line  
93 techniques like electrospray ionization (ESI)-MS (Nizkorodov et al., 2011; Laskin et al., 2012;  
94 Witkowski and Gierczak, 2013), have remained largely unavailable for CIMS (Fujii et al., 2001).

带格式的: 字体颜色: 自动设置

域代码已更改

95 Compared to I<sup>-</sup>, NO<sub>3</sub><sup>-</sup>, and acetate, which are generally more sensitive to more oxygenated  
96 organic compounds than to less oxygenated ones (Aljawhary et al., 2013; Lee et al., 2014,  
97 Hytinen et al., 2015; Iyer et al., 2016, Berndt et al., 2016), these metal cations are expected to be  
98 less selective toward oxygenated oxidized organic compounds and can be used be able to  
99 sensitively detect both less oxygenated oxidized (e.g. compounds containing only carbonyl  
100 groups) and highly oxygenated polar multi-functional organic species (Gao et al., 2010; Nguyen  
101 et al., 2010; Nizkorodov et al., 2011; Laskin et al., 2012; Witkowski and Gierczak, 2013; Zhao et  
102 al., 2015; Tu et al., 2016; Zhao et al., 2016; Zhang et al., 2017), and to form more strongly bound  
103 ion adducts. In addition, at present most CIMS techniques use a radioactive ion source such as  
104 Po-210 to produce the reagent ions, although more recently some utilize X-ray radiation,  
105 electrical discharge (Hirokawa et al., 2009; Yuan et al., 2016), or electron impact (Inomata and  
106 Hirokawa, 2017). Safety regulations for the transport and use of radioactive materials may limit  
107 the deployment of the instrument with a radioactive ion source in the field, while other methods  
108 may be less intense or lead to higher backgrounds.

带格式的: 字体颜色: 自动设置

域代码已更改

域代码已更改

域代码已更改

109 We have developed a non-radioactive reagent ion source that deploys a custom-built electrospray  
110 setup within an atmospheric pressure orthogonal ion-molecule reaction (IMR) chamber. The  
111 design of the IMR region is similar to that of the Cluster-CIMS developed by Eisele and  
112 coworkers (Zhao et al., 2010). The electrospray chemical ionization (ESCI) source is coupled to  
113 a HRTof-MS for characterization. We present the design and discuss the parameters most  
114 important for optimal performance of the ESCI source. Then, we assess its performance using  
115 the measurement of formic acid, IEPOX, nitric acid, and organic mixtures formed by ozonolysis  
116 of  $\alpha$ -pinene in a continuous-flow reaction chamber. Our results demonstrate that the ESCI source  
117 provides a potential alternative to radioactive and X-ray ion source and opens a new avenue for  
118 the generation of reagent ions such as Li<sup>+</sup>, Na<sup>+</sup>, K<sup>+</sup>, and so on, that were previously unavailable  
119 for CIMS.

域代码已更改

## 120 2. Experimental

## 121 2.1 Instrument description

122 A schematic of the ESCI module is shown in Figure 1. The electrospray setup contains a 15  $\mu\text{m}$   
123 inner diameter (ID) fused silica spray needle (PicoTip™) mounted within a cylindrical  
124 evaporation chamber through which a flow of ultra-high purity (UHP)  $\text{N}_2$  (referred to as the ion  
125 source flow) is passed to aid in the evaporation of the spray droplets and to transport ions into the  
126 IMR. Several spray needle diameters were tried (from 8 to 30  $\mu\text{m}$ ), with the 15  $\mu\text{m}$  giving the  
127 best combination of longevity and ion intensity. The emitting end of the spray needle is located 4  
128 mm from the distal wall of the evaporation chamber, which consists of a 13 mm ID stainless  
129 steel (SS) tube welded to the center of a circular SS aperture having a 4 mm diameter. The  
130 aperture forms the entrance into the IMR which is a portion of a 22 mm ID SS tube embedded in  
131 a Teflon block. The ion source flow enters the IMR through the aperture perpendicularly to the  
132 direction of a much larger sample flow, typically 10 to 20 standard liters per minute (slpm)  
133 drawn through the IMR by a pump, dry scroll vacuum pump (IDP-3, Agilent Technologies).  
134 Preliminary fluid dynamic simulations suggest that the mixed sample and ion source flow in the  
135 IMR remains laminar when the ratio of the ion source flow to sample flow is  $\leq 0.2$  and the  
136 overall Reynolds number for the sample flow is low (sample flow  $< 20$  slpm).

带格式的: 字体颜色: 自动设置

137 Ions are driven across the perpendicular sample flow to a SS capillary tube located on the  
138 opposite wall of the IMR by means of a 2 to 4 kV potential between the evaporation region lens  
139 and the capillary tube. The SS capillary projects 3.5 mm into the IMR and acts as the  
140 atmospheric pressure interface between the IMR and the vacuum chamber of a commercial  
141 HRTof-MS (Tofwerk AG, Thun, Switzerland), effectively dropping the atmospheric pressure to  
142 1.5 Torr in the first quadrupole of the MS, and resulting in a sample flow of  $\sim 270$  sccm into the  
143 MS. The HRTof-MS and its data acquisition procedures have been described in detail previously,  
144 (Junninen et al., 2010; Bertram et al., 2011; Lee et al., 2014). The evaporation tube, lens and  
145 IMR tube are electrically connected, while the mass spectrometer entrance capillary is  
146 electrically isolated from the IMR by a  $\sim 1$  mm thick jacket of Teflon.

带格式的: 字体颜色: 自动设置

带格式的: 字体颜色: 自动设置

域代码已更改

147 During operation, a dilute salt solution ( $\sim 0.05$  wt%) in HPLC-grade methanol (MEOH) is biased  
148 at the reservoir to  $\pm (2-5)$  kV depending on the ion mode by connecting a stainless steel rod  
149 immersed into the solution to a high voltage power supply  $\sim 3$  to  $5$  kV. At a given reservoir  
150 solution voltage ( $V_R$ ), the voltage applied to the evaporation tube and IMR ( $V_L$ ) was carefully  
151 tuned to get the best ion signals ( $S_{\text{max}}$ ), as well as the corresponding  $V_L$ , referred to as  $V_L(S_{\text{max}})$ .  
152 In the  $V_R$  range of 2-5 kV, a larger  $V_s$  (with a larger  $V_L(S_{\text{max}})$ ) gives a higher reagent ion signal.  
153 In order to obtain good ion signals, for most of the measurements performed in this study,  $V_R$   
154 values of 5 kV (corresponding  $V_L(S_{\text{max}}) = 2.8$  kV) and -5 kV (corresponding  $V_L(S_{\text{max}}) = -3.5$  kV)  
155 were used in the positive ion and negative ion modes, respectively. The reservoir is maintained at  
156 approximately 50 mbar above atmosphere using a commercial pressure controller (FLUIGENT,  
157 model MFCS-EZ) with 0.05 mbar precision. As a result, the salt solution is pushed through the  
158 fused silica capillary tube to the spray needle at a flow rate less than  $100 \text{ nL min}^{-1}$  by the  
159 pressure in the reservoir bottle.

带格式的: 字体颜色: 自动设置

带格式的: 字体颜色: 自动设置

带格式的: 字体颜色: 自动设置

160 Under laminar flow conditions, the reaction time between reagent ions and sampled trace gases  
161 in the IMR is mainly determined by the electric field-induced drift velocity of the reagent ions.  
162 For instance, for two reagent ions used in this study,  $\text{NO}_3^-$  and  $\text{Na}^+$ , the ion-molecule reaction  
163 time (i.e., ion drift time) in the IMR is estimated to be 0.5-1 ms and 0.4-0.7 ms, respectively,  
164 with an ion mobility of  $2.37 \text{ cm}^2 \text{ s}^{-1} \text{ V}^{-1}$  for  $\text{NO}_3^-$  (Ellis et al., 1978) and  $3.4 \text{ cm}^2 \text{ s}^{-1} \text{ V}^{-1}$  for  $\text{Na}^+$   
165 (Bohringer et al., 1987) under typical operation conditions (2-4 kV across the IMR). However,  
166 when using electrospray as a source and sampling ambient air of different humidity, the reagent  
167 ions can be solvated by methanol or water clusters (Horning et al., 1974; Garvey et al., 1994). As  
168 the ion mobility of solvated reagent ions is likely smaller than that for unsolvated reagent ions,  
169 the ion-molecule reaction time between solvated reagent ions and gas phase analytes in the IMR  
170 is expected to be longer than that estimated for the unsolvated ions. There was no evidence of  
171 protonated methanol clustering observed when electrospraying a methanolic solution of the  
172 described salts except at the extreme voltage differences between the lens and entrance capillary  
173 where it was likely a discharge developed. Although the reagent ion is likely solvated by  
174 methanol initially, the sensitivity of the ionization to various trace gases did not appear to be  
175 significantly affected in the present study.

带格式的: 上标

域代码已更改

域代码已更改

带格式的: 字体颜色: 自动设置

176 The ion source and sample flow rates can significantly affect the performance of the ion source.  
177 The ion source flow can aid in the generation and transport of the reagent ions into the IMR, but  
178 it may disrupt the initially laminar sample flow, especially when the sample flow is small.  
179 However, at large sample flows, the time for the ions to exit the IMR via the sample flow may be  
180 comparable to the ion drift time across the IMR at a constant potential. As a result, the sample  
181 flow may carry away the reagent ions as well as ion-molecule clusters, lowering the apparent  
182 ionization efficiency. Therefore, the ion source flow and sample flow need to be carefully  
183 optimized.

带格式的: 字体颜色: 自动设置

184 For comparison purposes, our prototype source was designed such that it could incorporate a  
185 commercial 10 mCi Po-210 inline ion source (NRD LLC) as in more typical low-pressure CIMS  
186 instruments used for atmospheric composition studies (see introduction). With  $\text{CH}_3\text{I}$  in UHP  $\text{N}_2$   
187 as a reagent ion source, this set up was able to produce  $0.6-1.8 \times 10^6$  cps of reagent ions at  
188 atmospheric pressure using an ion source flow rate of 1-2 slpm and a sample flow rate of 10 slpm,  
189 with  $>2$  kV potential across the IMR. Although the commercial Po-210 sources are not  
190 optimized for ion transmission at low flow rates and high pressures, this intensity is certainly  
191 suitable for use in field or laboratory studies.

## 192 2.2 Laboratory characterization

### 193 2.2.1 Generation of reagent ions and calibration gas standards

194 In this study, three negative (i.e.,  $\text{I}^-$ ,  $\text{NO}_3^-$ , and acetate) and four positive reagent ions (i.e.,  $\text{Li}^+$ ,  
195  $\text{Na}^+$ ,  $\text{K}^+$ , and  $\text{NH}_4^+$ ) were generated by electrospraying their precursor salt solutions prepared in  
196 HPLC grade MEOH (Fisher Scientific). Sodium iodide ( $\geq 99.5\%$ , EMD), sodium nitrate ( $\geq 99\%$ ,

197 Mallinckrodt), potassium acetate (AR(ACS), Macron), ammonium acetate (99.2%, Fisher  
198 chemical), and lithium chloride ( $\geq 99\%$ , Mallinckrodt) were used to produce  $\Gamma^-$  and  $\text{Na}^+$ ,  $\text{NO}_3^-$ ,  $\text{K}^+$   
199 and acetate,  $\text{NH}_4^+$ , and  $\text{Li}^+$  respectively. All the salts were used as received.

200 Three calibration gases, i.e., nitric acid ( $\text{HNO}_3$ ), isotope-labeled formic acid ( $\text{H}^{13}\text{COOH}$ ), and  
201 isoprene epoxydiols (*trans*- $\beta$ -IEPOX) were used to calibrate the instrument. Gases of nitric acid  
202 and formic acid were generated using a custom-built PTFE permeation tube containing  
203 respective acid liquids, kept constantly at  $40^\circ\text{C}$ . The permeation rate was determined  
204 gravimetrically. IEPOX vapor was generated by passing a flow of UHP  $\text{N}_2$  over  $\sim 200\ \mu\text{l}$  IEPOX  
205 solution in ethyl acetate kept in a glass bulb at room temperature. The concentration of IEPOX in  
206 the flow exiting the bulb was determined by an Iodide-adduct HRTof-CIMS employing a  
207 radioactive ion source, for which the sensitivity to IEPOX was calibrated using the method as  
208 described previously (Lee et al., 2014). These three gases are common in the atmosphere and  
209 span a range in their properties important for CIMS such as acidity, polarity, and size.

域代码已更改

#### 210 2.2.2 Optimization of operation conditions, calibration, and background determination

211 The influence of sample flow and ion source flow on the ion signals was systematically  
212 evaluated using  $\Gamma^-$  as the reagent ion. The room air was directly sampled into the IMR at a flow  
213 rate ranging from 2-20 standard liters per minute (slpm). At each sample flow rate, the ratio of  
214 ion source flow/sample flow is varied from 0.02-0.2. The  $\text{HNO}_3$  and  $\text{H}^{13}\text{COOH}$  gases were added  
215 to the sample flow during the optimization.

216 Calibrations with  $\text{HNO}_3$ ,  $\text{H}^{13}\text{COOH}$ , and IEPOX were performed using  $\Gamma^-$  reagent ions under  
217 optimized sample flow and ion source flow conditions. Atmospherically relevant concentrations  
218 of the calibration gases were obtained by varying the dilution of the source gas in UHP  $\text{N}_2$  prior  
219 to delivery in the sample flow. The observed ion signals as a function of gas concentration allow  
220 the determination of the instrument sensitivity. In addition, the sample flow was humidified to a  
221 wide range of relative humidity (0-80% RH, corresponding to water vapor pressure,  $P_{\text{H}_2\text{O}}$ , of 0-  
222 25 mbar) to explore the influence of water vapor on the instrument sensitivity. The determined  
223 sensitivities as well as the dependence on  $P_{\text{H}_2\text{O}}$  were compared to the measurements by a  
224 radioactive Iodide-adduct HRTof-CIMS. The background signals of the instrument were  
225 determined routinely by directly sampling dry UHP  $\text{N}_2$ .

#### 226 2.2.4 Chamber experiments of $\alpha$ -pinene ozonolysis

227 The capability of the instrument for characterizing atmospherically relevant complex organic  
228 systems was evaluated by measuring the oxidation products from  $\alpha$ -pinene ozonolysis using  
229 seven different reagent ions described above. Experiments of  $\alpha$ -pinene ozonolysis were carried  
230 out in a  $0.75\ \text{m}^3$  PTFE chamber operated in a continuous-flow mode at the University of  
231 Washington. The chamber was first flushed by 12 slpm of zero air generated by a Teledyne zero  
232 air generator (Model 701) for  $>72\ \text{h}$ . Ozone, generated by flowing ultra-zero air (Praxair) at 5  
233 sccm (standard cubic centimeter per minute) past a mercury lamp, was delivered to the chamber

234 during the zero air flushing.  $\alpha$ -Pinene was then added by flowing 100 sccm of UHP N<sub>2</sub> through a  
235 glass diffusion tube containing pure  $\alpha$ -pinene and kept in a methanol cold trap at -70 °C. The  
236 initial concentrations of O<sub>3</sub> and  $\alpha$ -pinene added in the chamber were approximately 75 and 110  
237 ppbv, respectively. The oxidation products formed in the chamber were sampled at 10 slpm by  
238 the HRTof-ESCIMS after 48 h of chamber equilibration.

### 239 3. Results and Discussion

#### 240 3.1 Ion source and sample flow optimization

241 Figure 2a shows an example using iodide reagent ions of ion signal dependence on the ion source  
242 flow rate during sampling of humid air ( $P_{H_2O} = 15$  mbar) at 10 slpm containing an added  
243 H<sup>13</sup>COOH standard. As expected, the reagent ion (I<sup>-</sup> and I(H<sub>2</sub>O)<sup>-</sup>) signals increase with  
244 increasing ion source flow. The increase of the signal for I(H<sup>13</sup>COOH)<sup>-</sup> is well correlated with  
245 that of the reagent ions. The positive effect of the ion source flow is likely due to more efficient  
246 evaporation and transport of reagent ions from the spray evaporation region into the IMR region.

247 Figure 2b shows the ion signals for I<sup>-</sup>, I(H<sub>2</sub>O)<sup>-</sup>, I(H<sup>13</sup>COOH)<sup>-</sup>, and I(HNO<sub>3</sub>)<sup>-</sup> observed during  
248 sampling of humid air ( $P_{H_2O} = 15$  mbar) containing H<sup>13</sup>COOH and HNO<sub>3</sub> standards at a sample  
249 flow rate ranging from 2-20 slpm. The corresponding ion source flow was controlled to always  
250 be 1/10 of the sample flow. All ion signals increase initially with the increase of the sample flow,  
251 reach maximum values at 12 slpm, and then decrease slightly with further increase of the sample  
252 flow. -At small sample flows, the time for the sample flow to pass through the IMR is long  
253 compared to electric field-induced ion drift time across the IMR region, and so the influence of  
254 the sample flow upon ion transit across IMR should be small. However, the corresponding  
255 increase of the ion source flow with the sample flow can promote the generation and  
256 transmission of reagent ions into the IMR, thus leading to the increase of ion signals. At large  
257 sample flows, the influence of the sample flow on the ion transit across IMR becomes significant  
258 and is no longer compensated by the enhancement in ion signals due to the increased ion source  
259 flow, hence resulting in a decrease in ion signals. Note that the same measurement was also  
260 performed at ion source flow/sample flow ratios ranging from 0.02-0.2. The trend of the ion  
261 signal versus the sample flow at each flow ratio is very similar to that shown in Figure 2b,  
262 though the absolute ion signal values are different.

263 For the characterizations and applications discussed below, the sample flow and ion source flow  
264 are kept at 10 slpm and 1 slpm, respectively as these are reasonable conditions for use on  
265 environmental simulation chambers and in field measurements. We note that the sample flow can  
266 be extended to up to 20 slpm without significant loss of ion signal, and the optimal ion source  
267 flow of 2 slpm is essentially the same UHP N<sub>2</sub> flow requirement for current Po-210 based ion  
268 sources (Lee et al., 2014). Further improvements in the spray environment and associated  
269 transfer optics will likely further minimize the ion source flow.

带格式的: 正文1, 段落间距段前: 12 磅, 段后: 12 磅

带格式的: 字体颜色: 自动设置

带格式的: 字体颜色: 自动设置

域代码已更改

270 3.2 Evidence of chemical ionization

271 Electrospray plumes not only ionize solvated analytes, but also are capable of ionizing gas phase  
272 species (Whitehouse et al., 1986; Chen et al., 1994), the latter termed secondary electrospray  
273 ionization (SESI) (Wu et al., 2000; Tam and Hill, 2004). SESI-MS has been demonstrated in the  
274 real-time analysis of a variety of gas phase analytes, including pharmaceuticals (Wu et al., 2000;  
275 Meier et al., 2012), explosives (Tam and Hill et al., 2004; Aernecke et al., 2015), human  
276 metabolites (Martínez-Lozano et al., 2011; García-Gómez et al., 2015), electronic cigarette  
277 vapors (García-Gómez et al., 2016), as well as volatile emissions from bacteria cultures (Zhu et  
278 al., 2010), food (Bean et al., 2015; Farrell et al., 2017), and plants (Barrios-Collado et al., 2016).  
279 In SESI, the electrospray plume and incoming sample flow intersect in the ionization region, and  
280 analyte ionization proceeds likely via interactions with both small charged droplets and  
281 electrospray-produced gas phase reagent ions (Wu et al., 2000). In the present study, by coupling  
282 the electrospray source to an orthogonal continuous-flow atmospheric pressure IMR region via  
283 an evaporation region, we separate the electrospray plume from the incoming samples to avoid  
284 SESI, and instead allow for gas-phase chemical ionization.

285 Under typical operating conditions, the sample flow likely transports any unevaporated droplets  
286 away from the effective ionization region in the IMR, thus largely isolating the electrospray  
287 plume from the incoming samples, making the ESCI source a chemical ionization source rather  
288 than secondary or extractive electrospray ionization (SESI or EESI) source. The evidence of the  
289 ESCI source being a chemical ionization source and not SESI or EESI is provided by monitoring  
290 the signal ratio of  $\text{NO}_3^-/\text{I}(\text{HNO}_3)^-$  when sampling gas phase  $\text{HNO}_3$  in the iodide mode. If the  
291 direct interaction between electrospray plume and incoming sample flow is important,  $\text{HNO}_3$   
292 dissolved in charged droplets can dissociate forming  $\text{H}^+$  and  $\text{NO}_3^-$ , leading to the generation of  
293  $\text{NO}_3^-$  ions in the negative ion mode. Therefore, a large signal ratio of  $\text{NO}_3^-/\text{I}(\text{HNO}_3)^-$  is expected.  
294 Figure 3 shows the signal ratio of  $\text{NO}_3^-/\text{I}(\text{HNO}_3)^-$  as a function of gas phase  $\text{HNO}_3$  concentration  
295 under dry and wet conditions observed in the iodide mode. The signal ratios of  $\text{NO}_3^-/\text{I}(\text{HNO}_3)^-$   
296 are significantly smaller than 0.01 at various  $\text{HNO}_3$  concentrations, suggesting the direct  
297 interaction of electrospray plume with incoming samples is not important in the ESCI source.

298 3.3 Time response of the atmospheric pressure IMR

299 The time response of ESCI source/atmospheric pressure orthogonal IMR design was determined  
300 using nitric acid standard in the iodide mode.  $\text{HNO}_3$  was delivered from a permeation tube using  
301 a small ( $< 100$  sccm) continuous flow UHP  $\text{N}_2$  through a 3 mm OD Teflon tube to the inlet of the  
302 orthogonal IMR. Figure 4 shows the changes in ion signal for  $\text{I}(\text{HNO}_3)^-$  upon placing the  $\text{HNO}_3$   
303 delivery line at the opening of a 10 cm length of 2.5 cm OD Teflon tubing serving as the inlet to  
304 the IMR or removing the delivery line away from the inlet. Tests were conducted at an ion  
305 source flow of 1 slpm and sample flow of 5 or 10 slpm. The increase and decay of  $\text{I}(\text{HNO}_3)^-$   
306 signal relative to that from  $\text{HNO}_3$  in the laboratory air give an e-folding time of about 1s for

带格式的: 字体颜色: 自动设置

带格式的: 字体颜色: 自动设置

带格式的: 下标

带格式的: 下标

带格式的: 下标

带格式的: 上标

带格式的: 下标

带格式的: 下标

带格式的: 上标

带格式的: 下标

307 [nitric acid under two different flow conditions. This time response value is comparable to or](#)  
308 [better than that for the low pressure IMR \(1 second to a few seconds\).](#)

### 309 3.2.4 Sensitivity to selected trace gases

310 To assess the performance of the HRTof-ESCIMS, we measured the sensitivity to HNO<sub>3</sub>,  
311 H<sup>13</sup>COOH, and IEPOX using I<sup>-</sup> as the reagent ion. The iodide-based CIMS has been widely used  
312 to detect atmospheric inorganic and organic compounds in previous studies (Huey et al., 1995;  
313 Kercher et al., 2009; Lee et al., 2014; Brophy and Farmer, 2015; Lee et al., 2016; Lopez-Hilfiker  
314 et al., 2016b), though almost exclusively at low pressure (20 – 80 mbar) as opposed to the  
315 atmospheric pressure (1013 mbar) implementation used here. The sensitivity of iodide-based  
316 CIMS to a given compound mainly depends on the polarity and hydrogen binding energy of a  
317 compound to the I<sup>-</sup> ion (Lee et al., 2014; Iyer et al., 2016). In the atmospheric pressure ESCIMS,  
318 the ion molecule reaction time ([a few ms](#)) is set by the electric field, and is up to a factor of 30 or  
319 more shorter than those ([30-120 ms](#)) in low-pressure CIMS instruments ([Bertram et al., 2011;](#)  
320 [Lee et al., 2014, Lopez-Hilfiker et al., 2016a](#)). The shorter reaction time should linearly lower  
321 sensitivities. However, the ion-molecule collision frequency is more than a factor of 10 higher in  
322 the atmospheric pressure ESCIMS for the same ambient concentrations of analytes. Thus, we  
323 would expect the ESCIMS sensitivities to be only slightly lower than those found in the low-  
324 pressure CIMS. It is possible that adduct formation is further stabilized by third-body effects and  
325 that the ESCIMS could in fact have higher sensitivities for some compounds forming weaker  
326 clusters.

327 Figure [3-5](#) shows the signals of I(HNO<sub>3</sub>)<sup>-</sup>, I(H<sup>13</sup>COOH)<sup>-</sup>, and I(IEPOX)<sup>-</sup> per million reagent ion  
328 count rate at different atmospherically relevant concentrations of the standards under dry and  
329 humid conditions. The signal response is linear within the investigated concentration range for  
330 all three trace gases, with the slope of the linear fit to the ion signals corresponding to the  
331 sensitivity per million reagent ion count rate. The HRTof-ESCIMS exhibits a sensitivity of 11,  
332 2.4, and 10 cps pptv<sup>-1</sup> to HNO<sub>3</sub>, HCOOH, and IEPOX, respectively, under dry conditions and 9.1,  
333 0.5, and 1.7 cps pptv<sup>-1</sup>, respectively, under humid conditions ( $P_{H_2O} = 14$  or 15 mbar). These  
334 sensitivities, and those that follow are given per million cps of reagent ion. Lee et al. (2014)  
335 explored the sensitivity of a low-pressure Iodide-adduct HRTof-CIMS equipped with a  
336 radioactive ion source to a number of atmospheric inorganic and organic compounds. They  
337 reported sensitivities to HNO<sub>3</sub>, HCOOH, and IEPOX of 4.0, 2.9, and 0.39 cps pptv<sup>-1</sup>,  
338 respectively, at 0.2 mbar water vapor pressure in IMR. Using the same instrument as used by Lee  
339 et al. (2014), we have more recently obtained higher values of sensitivities to HCOOH (7 cps  
340 pptv<sup>-1</sup>) and IEPOX (10 cps pptv<sup>-1</sup>) in the laboratory. Thus, the atmospheric-pressure ESCIMS  
341 and low-pressure CIMS approaches are fairly similar in response to the same compounds. The  
342 sensitivity difference in these calibrations is likely attributed to the differences in instrument  
343 parameters, including the configurations and pressures of the ion source and IMR, and the ion  
344 optic settings within the vacuum chamber that strongly affect ion transmission to the mass  
345 spectrometer.

域代码已更改

域代码已更改

带格式的: 字体颜色: 自动设置

带格式的: 字体颜色: 自动设置

346 The presence of water vapor can affect sensitivities, either by competing for I<sup>-</sup> ions, thus  
347 lowering the sensitivity, or by accommodating excess energy from the collision to stabilize the  
348 Iodide-molecule clusters, thereby increasing the sensitivity (Lee et al., 2014; Iyer et al., 2016).

349 ~~Water vapor may also affect sensitivities by changing the size distribution of reagent ion clusters  
350 and thus their residence time (ion-molecule reaction time) in the IMR. Moreover, water vapor  
351 can affect the transmission of soluble gases through sample tubing. It is difficult to evaluate the  
352 effect of changing cluster size distribution as the information regarding the distribution and ion  
353 mobility of the reagent ion clusters is currently unavailable. In the current configuration of the  
354 ESCIMS, it is also difficult to isolate the sample transfer effect separate these two effects  
355 experimentally, as done previously in low-pressure IMR regions by using separate delivery lines  
356 for calibrants and water vapor (Lee et al 2014). Thus, our results shown here reflect a  
357 combination of ionization efficiency, cluster distribution, and sample transfer aspects and the  
358 latter could be significant given the 1 m length of tubing used in these tests. Thus, our results  
359 shown here reflect both ionization efficiency and sample transfer aspects because the sample  
360 flow delivering the calibrants had to be humidified.~~

361 Figure 4-6 shows the dependence of the instrument sensitivities to HNO<sub>3</sub>, H<sup>13</sup>COOH, and IEPOX  
362 on the P<sub>H2O</sub> of the sample flow. The sensitivities to HNO<sub>3</sub>, H<sup>13</sup>COOH, and IEPOX increase  
363 initially with the addition of water vapor at lower P<sub>H2O</sub>, reach the maximum values at 4.1, 2.2,  
364 and 2.2 mbar, respectively, and then decrease with the further increase of P<sub>H2O</sub>. Compared to  
365 HNO<sub>3</sub> and H<sup>13</sup>COOH, the positive water vapor effect on the sensitivity at low P<sub>H2O</sub> for IEPOX is  
366 significantly smaller. Lee et al. (2014) investigated the effects of water vapor on the sensitivity  
367 of a low-pressure Iodide-adduct HRTOF-CIMS in the P<sub>H2O</sub> (water vapor pressure in IMR) range  
368 of 0-0.8 mbar, and found a positive water vapor dependence for the sensitivity to HNO<sub>3</sub> and an  
369 approximately inverse U-shaped dependence for the sensitivity to HCOOH. In general, the  
370 trends for the sensitivities to HNO<sub>3</sub> and HCOOH versus P<sub>H2O</sub> observed by Lee et al. are  
371 consistent with those at P<sub>H2O</sub> ≤ 4.1 mbar observed in the present study. In addition, recent  
372 measurements using the same low-pressure Iodide-adduct HRTOF-CIMS in our lab show that  
373 the addition of water vapor with P<sub>H2O</sub> of 0.26 Torr has no significant impacts on the sensitivity to  
374 IEPOX, consistent with the relatively weak humidity dependence of the sensitivity to IEPOX at  
375 low P<sub>H2O</sub> observed in the present study. The sharp decrease in the sensitivities at higher P<sub>H2O</sub> as  
376 seen in Figure 4-6 is therefore likely a result of the competitive consumption of I<sup>-</sup> ions by water  
377 vapor, which dominates over the kinetic stabilization effect of water for the ion-molecule clusters,  
378 as well as a larger wall partitioning in the ~50 cm sampling tube under these conditions.

### 379 3.3-5 Instrument backgrounds and detection limits

380 The background signals for the instrument arise mainly from the impurities in the electrospray  
381 solvent and the salts used for the generation of reagent ions, as well as the desorption of gas  
382 species adsorbed onto the wall of the sampling tube and IMR. The instrument backgrounds were  
383 routinely measured by sampling UHP N<sub>2</sub>. Figure 5-7 shows a typical high-resolution mass  
384 spectrum in the I<sup>-</sup> mode recorded when sampling UHP N<sub>2</sub>. The spectrum recorded during the

域代码已更改

带格式的: 字体颜色: 自动设置

带格式的: 字体颜色: 自动设置

带格式的: 字体颜色: 自动设置

385 addition of HNO<sub>3</sub>, H<sup>13</sup>COOH, and IEPOX to the UHP N<sub>2</sub> flow is also displayed for comparison.  
386 The typical backgrounds for HNO<sub>3</sub>, H<sup>13</sup>COOH, and IEPOX were measured to be 800, 240, and  
387 50 cps, respectively. It is noted that the instrument backgrounds can be reduced by using higher  
388 purity electrospray solvents and reagent ion precursor salts, or by using a larger sample flow that  
389 can dilute the background concentration of the species desorbed from the wall. Moreover, many  
390 experiments adding large concentrations of these standards to the sampling tube had been  
391 performed over months, and thus it is likely that these backgrounds are anomalously high.

392 Assuming the uncertainty in the signal and background follows Poisson counting statistics, the  
393 signal to noise (*S/N*) ratio can be determined from eq. (1) (Bertram et al., 2011):

$$\frac{S}{N} = \frac{C_f[X]t}{\sqrt{C_f[X]t + 2Bt}} \quad (1)$$

394 Where *C<sub>f</sub>* is the instrument sensitivity; [*X*] is the concentration for a trace gas; *B* is the  
395 background count rate; *t* is the integration time. We define the detection limit of the HRTof-  
396 ESCIMS for a trace gas as the concentration that gives rise to an *S/N* ratio of 3. Using the  
397 measured instrument sensitivities and backgrounds, we calculate a detection limit of 4.9, 12.5,  
398 and 1.4 pptv for HNO<sub>3</sub>, H<sup>13</sup>COOH, and IEPOX, respectively, for 5s averaging, in the  $\Gamma$  mode.  
399 These limits of detection are comparable to those for a low-pressure Iodide-adduct HRTof-  
400 CIMS in our lab (Lee et al., 2014).

### 401 3.4.6 Application to chamber studies of $\alpha$ -pinene ozonolysis

#### 402 3.4.6.1 Raw mass spectra

403 Gas mixtures formed by ozonolysis of  $\alpha$ -pinene in a steady-state chamber were used to assess the  
404 capabilities of this technique for characterizing complex organic systems of atmospheric  
405 relevance. Three negative ions (i.e.,  $\Gamma$ , NO<sub>3</sub><sup>-</sup>, acetate) and four positive ions (i.e., Li<sup>+</sup>, Na<sup>+</sup>, K<sup>+</sup>,  
406 NH<sub>4</sub><sup>+</sup>) were used as reagent ions for measurements. High resolution peak fitting was performed  
407 and reasonable molecular formulae were assigned for detected ions that have intensity higher  
408 than 5 cps in all seven ion modes. Many ions are present at < 5 cps, which were excluded from  
409 the high-resolution fittings to ease the number of identifications required for comparison of  
410 several different reagent ion spectra. Although these lower signal ions might be of importance to  
411 various mechanisms of particle growth or organic radical chemistry, identifying their  
412 compositions was deemed beyond the scope of this paper. Many ions are present at < 5 cps,  
413 which might be of importance to various mechanisms of particle growth or organic radical  
414 chemistry, but the compositions of these ions is beyond the scope of this paper. Overall, the  
415 results show that the ions observed in NO<sub>3</sub><sup>-</sup> and four positive ion modes are in the form of ion-  
416 molecule clusters, whereas those observed in  $\Gamma$  and acetate modes are either ion-molecule  
417 clusters or molecular ions. The iodide clusters can be easily distinguished from iodide-free  
418 molecular ions due to the large negative mass defects of iodide (Lee et al., 2014), although this

域代码已更改

带格式的: 字体颜色: 自动设置

带格式的: 字体颜色: 自动设置

带格式的: 字体颜色: 自动设置

419 advantage weakens at sufficiently high masses (> ~ 500 m/Q for a resolution of 5000). In  
420 contrast, broadly distinguishing between acetate-neutral clusters and deprotonated organic ions  
421 in the acetate mode remains a challenge when using non-isotopically labeled acetate as the  
422 reagent ion and operating the instrument in a cluster-transmitting mode with no comprehensive  
423 voltage scanning experiments (Lopez-Hilfiker et al., 2015; Brophy and Farmer, 2016), as is the  
424 case in the present study. As a result, the high-resolution ions observed in the acetate mode  
425 cannot be confidently assigned to  $\alpha$ -pinene ozonolysis products and are excluded from further  
426 discussions, whereas broadly distinguishing between acetate clusters and deprotonated molecule  
427 ions remains a challenge when not using isotopically labeled acetate as the reagent ion.  
428 Therefore, while chemical formulae for the ions can be obtained, their attribution to a product of  
429  $\alpha$ -pinene ozonolysis cannot be made with high confidence (Lopez-Hilfiker et al., 2015; Brophy  
430 and Farmer, 2016).

带格式的: 字体颜色: 自动设置

431 Examples of high-resolution mass spectra of  $\alpha$ -pinene ozonolysis products derived in  $\Gamma$  and  $\text{NO}_3^-$   
432 modes are given in Figure 6-8 and the spectra obtained in four positive ion modes are given in  
433 Figure 79. The iodide-mode mass spectrum of the ozonolysis products obtained here is overall  
434 similar to that obtained using the low-pressure Iodide-adduct HRTof-CIMS (see Figure S1 in the  
435 Supplement) as discussed previously (Lopez-Hilfiker et al., 2015). It can be seen that peaks  
436 assigned to monomeric products ( $\leq C_{10}$ ) are apparent in all ion modes, while peaks associated  
437 with dimeric species are evident only in the positive ion mode (discussed further below). Peak  
438 distributions in both monomer and dimer regions is very similar for  $\text{Li}^+$ ,  $\text{Na}^+$ ,  $\text{K}^+$ , and  $\text{NH}_4^+$ ,  
439 suggesting these positive ions likely have a similar selectivity to  $\alpha$ -pinene ozonolysis products. It  
440 is interesting to note that in negative ion modes, ion clusters of precursor salt molecules (e.g.,  
441  $\text{I}(\text{NaI})^-$  and  $\text{NO}_3(\text{NaNO}_3)_n^-$ ) were observed with high intensities. These ions can be used as  
442 excellent mass calibration species.

域代码已更改

### 443 3.46.2 Mass defect plots

444 To better compare the sensitivity and selectivity between this subset of negative and positive  
445 reagent ions, the mass defects of identified products are plotted against their exact mass for  $\Gamma$ ,  
446  $\text{NO}_3^-$ , and  $\text{Na}^+$  modes. Figure 8-10 shows the comparisons of mass defect plots between  $\Gamma$  (or  
447  $\text{NO}_3^-$ ) mode and  $\text{Na}^+$  mode. In the mass defect plots, the green, yellow, and purple open circles  
448 represent the products observed only in one ion mode and their size is proportional to the signal  
449 intensity of observed clusters. The blue open markers in the plots represent the products  
450 identified in both ion modes of comparison and their size is proportional to the square root of the  
451 pinic acid-normalized signal intensity ratio ( $R$ ) between the two ion modes:

$$R = \frac{S_{A^-,i}/S_{A^-,PA}}{S_{Na^+,i}/S_{Na^+,PA}} \quad (2)$$

452 Where,  $S_{A^-,i}$  and  $S_{A^-,PA}$  are the signal intensity of clusters for product  $i$  and pinic acid in  $\Gamma$  (or  
453  $\text{NO}_3^-$ ) mode, respectively;  $S_{Na^+,i}$  and  $S_{Na^+,PA}$  are the signal intensity of product  $i$  and pinic acid

454 in  $\text{Na}^+$  mode, respectively. As pinic acid ( $\text{C}_9\text{H}_{14}\text{O}_4$ ) is among the most abundant products  
455 | observed in  $\text{I}^-$ ,  $\text{NO}_3^-$ , and  $\text{Na}^+$  modes (see Figures 6-8 and 79), the value of  $R$  (i.e., the size of the  
456 markers relative to that for pinic acid (red solid circles)) can be an indicator of the relative  
457 sensitivity of  $\text{I}^-$  (or  $\text{NO}_3^-$ ) and  $\text{Na}^+$  to the oxidation products.

458 In the monomer region of the mass defect plots, the less oxidized products observed in both  
459 modes of comparison generally have a value of  $R \leq 1$  (the blue markers have sizes smaller than  
460 or close to that of pinic acid). Thus,  $\text{Na}^+$  is generally more sensitive to less oxidized species than  
461  $\text{I}^-$  and  $\text{NO}_3^-$ , and most of products observed only in the  $\text{Na}^+$  mode show very low oxygen contents  
462 ( $n_{\text{O}} \leq 3$ ). As many of these species have signal intensities larger than 1000 cps, their absence in  $\text{I}^-$   
463 and  $\text{NO}_3^-$  modes suggests that  $\text{I}^-$  and  $\text{NO}_3^-$  are extremely insensitive to these least oxidized  
464 species, in agreement with the observations in previous studies (Lee et al., 2014; Hyttinen et al.,  
465 2015; Iyer et al., 2016). In contrast, the more oxidized products observed in both modes of  
466 comparison show a wide range of  $R$  values (e.g,  $R \leq 1$  or  $R \geq 1$ , corresponding to the blue  
467 markers having sizes smaller or larger than that of pinic acid). This indicates that  $\text{I}^-$ ,  $\text{NO}_3^-$ , and  
468  $\text{Na}^+$  are all sensitive to more oxidized species but have different sensitivities to a specific species.  
469 In fact, some highly oxidized products having high oxygen contents ( $n_{\text{O}} \geq 5$ ) are observed only in  
470 one of these three ion modes. Note that most of these products have signal intensities lower than  
471 50 cps, suggesting that they likely have very low concentrations, which are below the detection  
472 limit in the other two modes.

473 The selectivity of  $\text{I}^-$  and  $\text{NO}_3^-$  toward more oxidized species as suggested here is consistent with  
474 the observations in previous studies (Lee et al., 2014; Berndt et al., 2016), which showed that  
475 these two reagent ions can have distinct sensitivities to the oxidized species having similar  
476 oxygen contents, depending on the identities and locations of the functional groups. It is clear in  
477 | Figure 8-10 that some very small species (e.g.,  $\text{CH}_2\text{O}_2$ ,  $\text{CH}_2\text{O}_3$ ,  $\text{C}_2\text{H}_2\text{O}_3$ , and  $\text{C}_2\text{H}_4\text{O}_3$ ) have a  
478 value of  $R$  significantly larger than 1, indicating that  $\text{I}^-$  and  $\text{NO}_3^-$  are markedly more sensitive to  
479 these small species than is  $\text{Na}^+$ .

480 Comparisons of the mass defect plots in the dimers region show a large difference in the  
481 detection of the gas-phase dimers between  $\text{I}^-$  (or  $\text{NO}_3^-$ ) and  $\text{Na}^+$  modes. These dimers have  
482 compositions ranging, for example, from  $\text{C}_{15}\text{H}_{26}\text{O}_3$  to  $\text{C}_{20}\text{H}_{32}\text{O}_7$ . We note that many of these  
483 dimers have been recently detected in the gas-phase using a low-pressure Iodide-adduct HRTof-  
484 CIMS in a boreal forest environment (Mohr et al., 2017). Thus, while the lower detection  
485 efficiency of dimers in this work using  $\text{I}^-$  or  $\text{NO}_3^-$  may be from differences in reagent ion  
486 sensitivities, we suspect that differences in ion optic settings between negative and positive ion  
487 modes that affect ion transmission efficiencies at large mass-to-charge ratios is a more likely  
488 explanation. These settings were not optimized in this work, and improvements to high mass  
489 transmission in negative ion mode are ongoing. Therefore, we refrain from concluding about the  
490 | relative detection efficiency of dimers in negative ion mode using the atmospheric pressure ESCI.

域代码已更改

491 Figure 11 shows boxplots for the O:C ratio of monomeric products from  $\alpha$ -pinene ozonolysis  
492 detected in  $\Gamma$ ,  $\text{NO}_3^-$ , and  $\text{Na}^+$  modes. The O:C values for all the percentiles observed in  $\Gamma$  and  
493  $\text{NO}_3^-$  modes are overall similar, whereas the corresponding values observed in  $\text{Na}^+$  mode are  
494 obviously smaller. In addition, more than half of products observed in the three modes have a  
495 O:C ratio larger than 0.8. These results are consistent with the observations from Figure 10,  
496 where  $\Gamma$ ,  $\text{NO}_3^-$ , and  $\text{Na}^+$  are all sensitive to highly oxygenated organics, but the former two  
497 reagent ions are insensitive to less oxygenated organics as compared to  $\text{Na}^+$ .

带格式的: 字体颜色: 自动设置

带格式的: 字体颜色: 自动设置

带格式的: 字体颜色: 自动设置

498 In summary, these comparisons suggest that there is not a reagent ion that captures all  
499 components of  $\alpha$ -pinene ozonolysis with equally high sensitivity. Therefore, to gain a  
500 comprehensive view on a complex organic system, a combination of reagent ions with different  
501 selectivity is needed.

### 502 3.46.3 Declustering scans

503 Ion-molecule clusters, depending on their binding energies, may break apart due to collision-  
504 induced dissociation (i.e., declustering) during transmission through the ion optics within the  
505 vacuum chamber. In general, clusters with stronger binding energies can more easily survive  
506 declustering in the vacuum chamber, thus the instrument likely has higher sensitivities to the  
507 corresponding analytes, and the observed sensitivities should be closer to those calculated by  
508 ion-molecule collision rates. Declustering scanning, which is performed by systematically  
509 increasing the voltage difference ( $\Delta V$ ) between first and the second quadrupole sections of the  
510 MS, allows for insights into the binding energies of clusters (Lopez-Hilfiker et al., 2016a).

511 Figure 9-12 shows the declustering scans of clusters containing  $\text{C}_{10}\text{H}_{16}\text{O}_{2-8}$  and  $\text{C}_9\text{H}_{14}\text{O}_{3-8}$   
512 products in  $\Gamma$  and  $\text{NO}_3^-$  modes. It is clear that, with the increase of electrical field strength, the  
513 cluster signals for products having higher oxygen contents generally decay more slowly than  
514 those having lower oxygen contents. This is consistent with the fact that  $\Gamma$  and  $\text{NO}_3^-$  ions  
515 generally bind more strongly to compounds containing more hydroxy or hydroperoxy moieties  
516 (Lee et al., 2014; Hyttinen et al., 2015; Iyer et al., 2016). We note that the trends of decay for  
517  $\text{C}_{10}\text{H}_{16}\text{O}_{2-8}$  iodide clusters are in excellent agreement with previous measurements using a low-  
518 pressure iodide-adduct HRTof-CIMS (Lopez-Hilfiker et al., 2016a).

域代码已更改

域代码已更改

519 Declustering scans in  $\text{Li}^+$ ,  $\text{Na}^+$ ,  $\text{K}^+$ , and  $\text{NH}_4^+$  modes show that the cluster signals for the most  
520 abundant monomeric products such as  $\text{C}_{10}\text{H}_{16}\text{O}_{2-5}$  and  $\text{C}_9\text{H}_{14}\text{O}_{2-5}$  increase initially with  
521 increasing  $\Delta V$  and then decrease with further increase of  $\Delta V$ . The reason for the initial increase  
522 in cluster signals is unclear, but might involve secondary ion chemistry and/or slight changes in  
523 ion transmission efficiency of the instrument.~~The initial increase in cluster signals may be~~  
524 ~~associated with ion transmission efficiency of the instrument. As the small positive reagent ions~~  
525 ~~have very low transmission efficiencies through the ion optics, the concentration of the reagent~~  
526 ~~ions in the vacuum chamber may be low. As a result, the declustering of reagent ion-water and-~~  
527 ~~precursor salt molecule clusters may greatly increase the concentration of reagent ions in the~~

带格式的: 字体颜色: 自动设置

528 ~~vacuum chamber. These reagent ions may quickly bind to the neutral oxidation products that are~~  
529 ~~present in larger abundance, leading to the increase of their cluster signals.~~ Here, we use the  
530 declustering scans of dimers instead of C<sub>9</sub> and C<sub>10</sub> monomers to compare the binding energies of  
531 four positive reagent ions.

532 As can be seen in Figure ~~40~~13, the decay rate of the cluster signals in four positive ion modes  
533 follows the order: NH<sub>4</sub><sup>+</sup> > K<sup>+</sup> > Na<sup>+</sup> > Li<sup>+</sup>. This indicates an order of Li<sup>+</sup> > Na<sup>+</sup> > K<sup>+</sup> > NH<sub>4</sub><sup>+</sup> for  
534 the binding energies of the clusters, consistent with expectations from charge density  
535 considerations. In each ion mode, the cluster signals for smaller dimers generally decay more  
536 slowly than those for larger dimers, suggesting these positive ions can more strongly bind to the  
537 smaller dimers, likely due to the higher polarity or the smaller steric effect for smaller dimers. It  
538 is worth noting that in the Li<sup>+</sup> mode, these dimer ions have ΔV<sub>50</sub> values of ~ 15V, suggesting  
539 they are very strongly bound, with a binding enthalpy of ~ 70 kcal/mol according to the  
540 relationship between ΔV<sub>50</sub> and cluster binding energies determined by Lopez-Hilfiker et al.  
541 (2016a). ~~It is worth noting that none of the clusters signals drop with the increase of ΔV up to 10~~  
542 ~~and 6 V in Li<sup>+</sup> and Na<sup>+</sup> modes, respectively. This behavior implies these dimers are most likely~~  
543 ~~covalently bound species formed during α-pinene ozonolysis, rather than nonecovalently bound~~  
544 ~~species formed due to ion induced clustering in the instrument, which are not expected to survive~~  
545 ~~at strong declustering strengths. To our knowledge, this result is the first direct confirmation that~~  
546 ~~these dimeric products are strongly bound, providing important support for the interpretation that~~  
547 ~~the detected ions represent real gas phase products of α-pinene oxidation (Ehn et al., 2012; Zhao~~  
548 ~~et al., 2013; Ehn et al., 2014; Kristensen et al., 2016; Trostl et al., 2016; Mohr et al., 2017)~~

带格式的: 字体颜色: 自动设置

带格式的: 字体颜色: 自动设置

域代码已更改

#### 549 4. Conclusion

550 We report an electrospray chemical ionization (ESCI) source coupled to a HRToF-MS for the  
551 real-time online measurement of atmospheric organic and inorganic species in the gas-phase.  
552 The ESCI source is unique in that it does not rely on radioactive materials or X-ray radiation that  
553 are subject to safety regulations, and allows the production of reagent ions (e.g., alkaline cations)  
554 that are not available in current CIMS techniques. Calibration experiments using nitric acid,  
555 formic acid, and IEPOX gas standards show that the HRToF-ESCIMS using iodide reagent ions  
556 has sensitivities and limits of detection comparable to those obtained for a low-pressure Iodide-  
557 adduct HRToF-CIMS using a radioactive ion source. The detection of oxidized organic  
558 compounds formed from α-pinene ozonolysis in a chamber using seven different reagent ions  
559 (e.g., I, NO<sub>3</sub><sup>-</sup>, acetate, Li<sup>+</sup>, Na<sup>+</sup>, K<sup>+</sup>, and NH<sub>4</sub><sup>+</sup>) shows different selectivities for these reagent ions  
560 and expected ion-adduct binding energy trends. The data demonstrate the capability of this  
561 technique for comprehensively characterizing complex organic systems using a combination of  
562 reagent ions.

563 The ESCI source presented here is in its early stages of development. Continued characterization  
564 of the sensitivity and selectivity of different reagent ions, especially their dependence on  
565 humidity are needed. Further optimizations of the ion source are also required to improve its

566 performance especially the long-time stability, which is particularly important for field  
567 applications. Versions of our prototype source allowed 10 to 24 hours of continuous operation  
568 before ion signal degraded, which is certainly suitable for many laboratory experiment durations.  
569 A short immersion of the spray tip into HPLC grade MEOH was enough to return to the same  
570 ion signal for another 10 to 24 hours, suggesting the reason was simply salt build-up on the spray  
571 needle tip altering the spray characteristics. Thus, it is likely that more dilute spray solutions,  
572 shorter spray needle tips, a conventional coaxial sheath gas flow around the needle tip, and off-  
573 axis spray geometry would greatly improve source stability. Moreover, shifting the spray source  
574 further upstream of the entrance capillary would increase ion-molecule reaction times and thus  
575 sensitivity, as in Zhao et al. (2013). Finally, applying a dry UHP N<sub>2</sub> counter flow at the mass  
576 spectrometer entrance capillary would prevent ambient particles and possible charged spray  
577 droplets that are not completely evaporated from entering and blocking the capillary tube. This  
578 counter flow could also prevent free water molecules entering the vacuum chamber and promote  
579 the dissociation of reagent ion-water clusters, which may lead to an increase of the instrument  
580 sensitivity, especially in positive ion mode.

581

## 582 Acknowledgement

583 This work was supported by the National Science Foundation (CHE-1404573). Jeremy Chan  
584 acknowledges the support of the University of Washington Royalty Research Fund (Grant 65-  
585 7716). [Felipe D. Lopez-Hilfiker and Jay G. Slowik acknowledge the support from the Swiss](#)  
586 [National Science Foundation \(Grant BSSG10 155846\)](#). We are grateful to Dennis Canuelle, the  
587 instrument maker, for help in designing and building the ESCI source.

588

## 589 References

- 590 Aernecke, M. J., Mendum, T., Geurtsen, G., Ostrinskaya, A., and Kunz, R. R.: Vapor Pressure of  
591 Hexamethylene Triperoxide Diamine (HMTD) Estimated Using Secondary Electrospray  
592 Ionization Mass Spectrometry, *J. Phys. Chem. A*, 119, 11514-11522, 2015.
- 593 Aljawhary, D., Lee, A. K. Y., and Abbatt, J. P. D.: High-resolution chemical ionization mass  
594 spectrometry (ToF-CIMS): application to study SOA composition and processing, *Atmos.*  
595 *Meas. Tech.*, 6, 3211-3224, doi:10.5194/amt-6-3211-2013, 2013.
- 596 Barrios-Collado, C., Garcia-Gomez, D., Zenobi, R., Vidal-de-Miguel, G., Ibanez, A. J., and  
597 Sinues, P. M. L.: Capturing in Vivo Plant Metabolism by Real-Time Analysis of Low to  
598 High Molecular Weight Volatiles, *Anal. Chem.*, 88, 2406-2412,  
599 doi:10.1021/acs.analchem.5b04452, 2016.
- 600 Bean, H. D., Mellors, T. R., Zhu, J. J., and Hill, J. E.: Profiling Aged Artisanal Cheddar Cheese  
601 Using Secondary Electrospray Ionization Mass Spectrometry, *J. Agric. Food Chem.*, 63,  
602 4386-4392, doi:10.1021/jf5063759, 2015.

域代码已更改

603 Berndt, T., Richters, S., Jokinen, T., Hyttinen, N., Kurten, T., Otkjaer, R. V., Kjaergaard, H. G.,  
604 Stratmann, F., Herrmann, H., Sipila, M., Kulmala, M., and Ehn, M.: Hydroxyl radical-  
605 induced formation of highly oxidized organic compounds, *Nat Commun*, 7, 13677, 2016.  
606 Bertram, T. H., Kimmel, J. R., Crisp, T. A., Ryder, O. S., Yataavelli, R. L. N., Thornton, J. A.,  
607 Cubison, M. J., Gonin, M., and Worsnop, D. R.: A field-deployable, chemical ionization  
608 time-of-flight mass spectrometer, *Atmos. Meas. Tech.*, 4, 1471-1479, 2011.  
609 Bohringer, H., Fahey, D. W., Lindinger, W., Howorka, F., Fehsenfeld, F. C., and Albritton, D. L.:  
610 Mobilities of several mass-identified positive and negative ions in air, *Int. J. Mass*  
611 *Spectrom. Ion Processes*, 81, 45-65, 1987.  
612 Breitenlechner, M., Fischer, L., Hainer, M., Heinritzi, M., Curtius, J., and Hansel, A.: PTR3: An  
613 Instrument for Studying the Lifecycle of Reactive Organic Carbon in the Atmosphere,  
614 *Anal. Chem.*, 89, 5825-5832, doi:10.1021/acs.analchem.6b05110, 2017.  
615 Brophy, P., and Farmer, D. K.: A switchable reagent ion high resolution time-of-flight chemical  
616 ionization mass spectrometer for real-time measurement of gas phase oxidized species:  
617 characterization from the 2013 southern oxidant and aerosol study, *Atmos. Meas. Tech.*,  
618 8, 2945-2959, 2015.  
619 Brophy, P., and Farmer, D. K.: Clustering, methodology, and mechanistic insights into acetate  
620 chemical ionization using high-resolution time-of-flight mass spectrometry, *Atmos. Meas.*  
621 *Tech.*, 9, 3969-3986, doi:10.5194/amt-9-3969-2016, 2016.  
622 Chen, Y. H., Hill, H. H., and Wittmer, D. P.: Analytical Merit of Electrospray Ion Mobility  
623 Spectrometry as a Chromatographic Detector, *J. Microcolumn Separations*, 6, 515-524,  
624 doi:10.1002/mcs.1220060511, 1994.  
625 Crounse, J. D., McKinney, K. A., Kwan, A. J., and Wennberg, P. O.: Measurement of gas-phase  
626 hydroperoxides by chemical ionization mass spectrometry, *Anal. Chem.*, 78, 6726-6732,  
627 2006.  
628 Ehn, M., Kleist, E., Junninen, H., Petaja, T., Lonn, G., Schobesberger, S., Dal Maso, M.,  
629 Trimborn, A., Kulmala, M., Worsnop, D. R., Wahner, A., Wildt, J., and Mentel, T. F.:  
630 Gas phase formation of extremely oxidized pinene reaction products in chamber and  
631 ambient air, *Atmos. Chem. Phys.*, 12, 5113-5127, 2012.  
632 Ehn, M., Thornton, J. A., Kleist, E., Sipila, M., Junninen, H., Pullinen, I., Springer, M., Rubach,  
633 F., Tillmann, R., Lee, B., Lopez-Hilfiker, F., Andres, S., Acir, I. H., Rissanen, M.,  
634 Jokinen, T., Schobesberger, S., Kangasluoma, J., Kontkanen, J., Nieminen, T., Kurten, T.,  
635 Nielsen, L. B., Jorgensen, S., Kjaergaard, H. G., Canagaratna, M., Dal Maso, M., Berndt,  
636 T., Petaja, T., Wahner, A., Kerminen, V. M., Kulmala, M., Worsnop, D. R., Wildt, J., and  
637 Mentel, T. F.: A large source of low-volatility secondary organic aerosol, *Nature*, 506,  
638 476-479, doi:10.1038/nature13032, 2014.  
639 Ellis, H. W., McDaniel, E. W., Albritton, D. L., Viehland, L. A., Lin, S. L., and Mason, E. A.:  
640 Transport properties of gaseous ions over a wide energy range. Part II, *At. Data Nucl.*  
641 *Data Tables*, 22, 179-217, 1978.  
642 Farrell, R. R., Fahrretrapp, J., Garcia-Gomez, D., Martinez-Lozano, P., Zenobi, R.: Rapid  
643 fingerprinting of grape volatile composition using secondary electrospray ionization  
644 orbitrap mass spectrometry: A preliminary study of grape ripening, *Food Control*, 81,  
645 107-112, 2017.  
646 Finlayson-Pitts, B. J., and Pitts, J. N.: Chemistry of the upper and lower atmosphere: theory,  
647 experiments, and applications, Academic Press, San Diego, 2000.

648 Fortner, E. C., Zhao, J., and Zhang, R. Y.: Development of ion drift-chemical ionization mass  
649 spectrometry, *Anal. Chem.*, 76, 5436-5440, 2004.

650 Fujii, T., Selvin, P. C., Sablier, M., and Iwase, K.: Lithium ion attachment mass spectrometry for  
651 on-line analysis of trace components in air: direct introduction, *Int. J. Mass Spectrom.*,  
652 209, 39-45, 2001.

653 Gao, Y. Q., Hall, W. A., and Johnston, M. V.: Molecular composition of monoterpene secondary  
654 organic aerosol at low mass loading, *Environ. Sci. Technol.*, 44, 7897-7902,  
655 doi:10.1021/Es101861k, 2010.

656 Garcia-Gomez, D., Bregy, L., Barrios-Collado, C., Vidal-de-Miguel, G., and Zenobi, R.: Real-  
657 Time High-Resolution Tandem Mass Spectrometry Identifies Furan Derivatives in  
658 Exhaled Breath, *Anal. Chem.*, 87, 6919-6924, doi:10.1021/acs.analchem.5b01509, 2015.

659 Garcia-Gomez, D., Gaisl, T., Barrios-Collado, C., Vidal-de-Miguel, G., Kohler, M., and Zenobi,  
660 R.: Real-Time Chemical Analysis of E-Cigarette Aerosols By Means Of Secondary  
661 Electrospray Ionization Mass Spectrometry, *Chem. Eur. J.*, 22, 2452-2457, 2016.

662 Garvey, J. F., Herron, W. J., and Vaidyanathan, G.: Probing the Structure and Reactivity of  
663 Hydrogen-Bonded Clusters of the Type  $\{M\}_n\{H_2O\}H^+$ , via the Observation of Magic  
664 Numbers, *Chem. Rev.*, 94, 1999-2014, doi:10.1021/Cr00031a011, 1994.

665 Goldstein, A. H., and Galbally, I. E.: Known and unexplored organic constituents in the earth's  
666 atmosphere, *Environ. Sci. Technol.*, 41, 1514-1521, doi:10.1021/Es072476p, 2007.

667 Hearn, J. D., and Smith, G. D.: A chemical ionization mass spectrometry method for the online  
668 analysis of organic aerosols, *Anal. Chem.*, 76, 2820-2826, 2004.

669 Hirokawa, J., Kato, T., and Mafune, F.: In situ measurements of atmospheric nitrous acid by  
670 chemical ionization mass spectrometry using chloride ion transfer reactions, *Anal. Chem.*,  
671 81, 8380-8386, 2009.

672 Horning, E. C., Carroll, D. I., Dzidic, I., Haegele, K. D., Horning, M. G., and Stillwell, R.: Liquid  
673 Chromatograph Mass Spectrometer-Computer Analytical Systems - Continuous-Flow  
674 System Based on Atmospheric-Pressure Ionization Mass-Spectrometry, *J. Chromatogr.*,  
675 99, 13-21, 1974.

676 Huey, L. G., Hanson, D. R., and Howard, C. J.: Reactions of  $SF_6^-$  and I<sup>-</sup> with Atmospheric Trace  
677 Gases, *J. Phys. Chem.*, 99, 5001-5008, 1995.

678 Huey, L. G.: Measurement of trace atmospheric species by chemical ionization mass  
679 spectrometry: Speciation of reactive nitrogen and future directions, *Mass Spectrom. Rev.*,  
680 26, 166-184, doi:10.1002/mas.20118, 2007.

681 Hyttinen, N., Kupiainen-Maatta, O., Rissanen, M. P., Muuronen, M., Ehn, M., and Kurten, T.:  
682 Modeling the charging of highly oxidized cyclohexene ozonolysis products using nitrate-  
683 based chemical ionization, *J. Phys. Chem. A*, 119, 6339-6345,  
684 doi:10.1021/acs.jpca.5b01818, 2015.

685 Inomata, S., and Hirokawa, J.: Non-radioactive chemical ionization mass spectrometry using  
686 acetic acid-acetate cluster as a reagent ion for the real-time measurement of acids and  
687 hydroperoxides, *Chem. Lett.*, 46, 38-41, 2017.

688 Iyer, S., Lopez-Hilfiker, F., Lee, B. H., Thornton, J. A., and Kurten, T.: Modeling the detection  
689 of organic and inorganic compounds using iodide-based chemical ionization, *J. Phys.*  
690 *Chem. A*, 120, 576-587, doi:10.1021/acs.jpca.5b09837, 2016.

691 Jokinen, T., Berndt, T., Makkonen, R., Kerminen, V. M., Junninen, H., Paasonen, P., Stratmann,  
692 F., Herrmann, H., Guenther, A. B., Worsnop, D. R., Kulmala, M., Ehn, M., and Sipila, M.:  
693 Production of extremely low volatile organic compounds from biogenic emissions:

694 Measured yields and atmospheric implications, *Proc. Natl. Acad. Sci. U. S. A.*, 112,  
695 7123-7128, 2015.

696 Junninen, H., Ehn, M., Petaja, T., Luosujarvi, L., Kotiaho, T., Kostianen, R., Rohner, U., Gonin,  
697 M., Fuhrer, K., Kulmala, M., and Worsnop, D. R.: A high-resolution mass spectrometer  
698 to measure atmospheric ion composition, *Atmos. Meas. Tech.*, 3, 1039-1053, 2010.

699 Kercher, J. P., Riedel, T. P., and Thornton, J. A.: Chlorine activation by N<sub>2</sub>O<sub>5</sub>: simultaneous, in  
700 situ detection of ClNO<sub>2</sub> and N<sub>2</sub>O<sub>5</sub> by chemical ionization mass spectrometry, *Atmos.*  
701 *Meas. Tech.*, 2, 193-204, 2009.

702 Kim, M. J., Zoerb, M. C., Campbell, N. R., Zimmermann, K. J., Blomquist, B. W., Huebert, B. J.,  
703 and Bertram, T. H.: Revisiting benzene cluster cations for the chemical ionization of  
704 dimethyl sulfide and select volatile organic compounds, *Atmos. Meas. Tech.*, 9, 1473-  
705 1484, 2016.

706 Kristensen, K., Watne, A. K., Hammes, J., Lutz, A., Petaja, T., Hallquist, M., Bilde, M., and  
707 Glasius, M.: High-Molecular weight dimer esters are major products in aerosols from  $\alpha$ -  
708 pinene ozonolysis and the boreal forest, *Environ. Sci. Technol. Lett.*, 3, 280-285,  
709 doi:10.1021/acs.estlett.6b00152, 2016.

710 Laskin, A., Laskin, J., and Nizkorodov, S. A.: Mass spectrometric approaches for chemical  
711 characterisation of atmospheric aerosols: critical review of the most recent advances,  
712 *Environ. Chem.*, 9, 163-189, doi:10.1071/EN12052, 2012.

713 Lee, B. H., Lopez-Hilfiker, F. D., Mohr, C., Kurten, T., Worsnop, D. R., and Thornton, J. A.: An  
714 Iodide-adduct high-resolution time-of-flight chemical-ionization mass spectrometer:  
715 Application to atmospheric inorganic and organic compounds, *Environ. Sci. Technol.*, 48,  
716 6309-6317, doi:10.1021/es500362a, 2014.

717 Lee, B. H., Mohr, C., Lopez-Hilfiker, F. D., Lutz, A., Hallquist, M., Lee, L., Romer, P., Cohen,  
718 R. C., Iyer, S., Kurten, T., Hu, W. W., Day, D. A., Campuzano-Jost, P., Jimenez, J. L.,  
719 Xu, L., Ng, N. L., Guo, H. Y., Weber, R. J., Wild, R. J., Brown, S. S., Koss, A., de Gouw,  
720 J., Olson, K., Goldstein, A. H., Seco, R., Kim, S., McAvey, K., Shepson, P. B., Starn, T.,  
721 Baumann, K., Edgerton, E. S., Liu, J. M., Shilling, J. E., Miller, D. O., Brune, W.,  
722 Schobesberger, S., D'Ambro, E. L., and Thornton, J. A.: Highly functionalized organic  
723 nitrates in the southeast United States: Contribution to secondary organic aerosol and  
724 reactive nitrogen budgets, *Proc. Natl. Acad. Sci. U. S. A.*, 113, 1516-1521,  
725 doi:10.1073/pnas.1508108113, 2016.

726 Lopez-Hilfiker, F. D., Mohr, C., Ehn, M., Rubach, F., Kleist, E., Wildt, J., Mentel, T. F., Lutz, A.,  
727 Hallquist, M., Worsnop, D., and Thornton, J. A.: A novel method for online analysis of  
728 gas and particle composition: description and evaluation of a Filter Inlet for Gases and  
729 AEROSols (FIGAERO), *Atmos. Meas. Tech.*, 7, 983-1001, doi:10.5194/amt-7-983-2014,  
730 2014.

731 Lopez-Hilfiker, F. D., Mohr, C., Ehn, M., Rubach, F., Kleist, E., Wildt, J., Mentel, T. F.,  
732 Carrasquillo, A. J., Daumit, K. E., Hunter, J. F., Kroll, J. H., Worsnop, D. R., and  
733 Thornton, J. A.: Phase partitioning and volatility of secondary organic aerosol  
734 components formed from alpha-pinene ozonolysis and OH oxidation: the importance of  
735 accretion products and other low volatility compounds, *Atmos. Chem. Phys.*, 15, 7765-  
736 7776, doi:10.5194/acp-15-7765-2015, 2015.

737 Lopez-Hilfiker, F. D., Iyer, S., Mohr, C., Lee, B. H., D'Ambro, E. L., Kurten, T., and Thornton, J.  
738 A.: Constraining the sensitivity of iodide adduct chemical ionization mass spectrometry

739 to multifunctional organic molecules using the collision limit and thermodynamic  
740 stability of iodide ion adducts, *Atmos. Meas. Tech.*, 9, 1505-1512, 2016a.

741 Lopez-Hilfiker, F. D., Mohr, C., D'Ambro, E. L., Lutz, A., Riedel, T. P., Gaston, C. J., Iyer, S.,  
742 Zhang, Z., Gold, A., Surratt, J. D., Lee, B. H., Kurten, T., Hu, W. W., Jimenez, J.,  
743 Hallquist, M., and Thornton, J. A.: Molecular Composition and Volatility of Organic  
744 Aerosol in the Southeastern US: Implications for IEPOX Derived SOA, *Environ. Sci.*  
745 *Technol.*, 50, 2200-2209, doi:10.1021/acs.est.5b04769, 2016b.

746 Martinez-Lozano, P., Zingaro, L., Finiguerra, A., and Cristoni, S.: Secondary electrospray  
747 ionization-mass spectrometry: breath study on a control group, *J. Breath Res.*, 5,  
748 doi:10.1088/1752-7155/5/1/016002, 2011.

749 Meier, L., Berchtold, C., Schmid, S., and Zenobi, R.: Sensitive detection of drug vapors using an  
750 ion funnel interface for secondary electrospray ionization mass spectrometry, *J. Mass*  
751 *Spectrom.*, 47, 555-559, doi:10.1002/jms.2982, 2012.

752 Mohr, C., Lopez-Hilfiker, F. D., Yli-Juuti, T., Heitto, A., Lutz, A., Hallquist, M., D'Ambro, E. L.,  
753 Rissanen, M. P., Hao, L. Q., Schobesberger, S., Kulmala, M., Mauldin III, R. L., Ulla  
754 Makkonen, U., Sipilä, M., Petäjä, T., Thornton, J. A.: Ambient observations of dimers  
755 from terpene oxidation in the gas-phase: implications for new particle formation and  
756 growth, *Geophys. Res. Lett.*, doi: 10.1002/2017GL072718, 2017.

757 Nguyen, T. B., Bateman, A. P., Bones, D. L., Nizkorodov, S. A., Laskin, J., and Laskin, A.:  
758 High-resolution mass spectrometry analysis of secondary organic aerosol generated by  
759 ozonolysis of isoprene, *Atmos. Environ.*, 44, 1032-1042, 2010.

760 Nizkorodov, S. A., Laskin, J., and Laskin, A.: Molecular chemistry of organic aerosols through  
761 the application of high resolution mass spectrometry, *Phys. Chem. Chem. Phys.*, 13,  
762 3612-3629, doi:10.1039/c0cp02032j, 2011.

763 Nowak, J. B., Huey, L. G., Eisele, F. L., Tanner, D. J., Mauldin, R. L., Cantrell, C., Kosciuch, E.,  
764 and Davis, D. D.: Chemical ionization mass spectrometry technique for detection of  
765 dimethylsulfoxide and ammonia, *J. Geophys. Res.*, 107, doi:10.1029/2001jd001058, 2002.

766 Noziere, B., Kaberer, M., Claeys, M., Allan, J., D'Anna, B., Decesari, S., Finessi, E., Glasius, M.,  
767 Grgic, I., Hamilton, J. F., Hoffmann, T., Iinuma, Y., Jaoui, M., Kahno, A., Kampf, C. J.,  
768 Kourtchev, I., Maenhaut, W., Marsden, N., Saarikoski, S., Schnelle-Kreis, J., Surratt, J.  
769 D., Szidat, S., Szmigielski, R., and Wisthaler, A.: The Molecular Identification of  
770 Organic Compounds in the Atmosphere: State of the Art and Challenges, *Chem. Rev.*,  
771 115, 3919-3983, doi:10.1021/cr5003485, 2015.

772 Praplan, A. P., Schobesberger, S., Bianchi, F., Rissanen, M. P., Ehn, M., Jokinen, T., Junninen,  
773 H., Adamov, A., Amorim, A., Dommen, J., Duplissy, J., Hakala, J., Hansel, A., Heinritzi,  
774 M., Kangasluoma, J., Kirkby, J., Krapf, M., Kurten, A., Lehtipalo, K., Riccobono, F.,  
775 Rondo, L., Sarnela, N., Simon, M., Tome, A., Trostl, J., Winkler, P. M., Williamson, C.,  
776 Ye, P., Curtius, J., Baltensperger, U., Donahue, N. M., Kulmala, M., and Worsnop, D. R.:  
777 Elemental composition and clustering behaviour of alpha-pinene oxidation products for  
778 different oxidation conditions, *Atmos. Chem. Phys.*, 15, 4145-4159, 2015.

779 Seinfeld, J. H., and Pandis, S. N.: *Atmospheric chemistry and physics: from air pollution to*  
780 *climate change*, 2nd ed., J. Wiley, Hoboken, N.J., 2006.

781 Smith, J. N., Moore, K. F., McMurry, P. H., and Eisele, F. L.: Atmospheric measurements of  
782 sub-20 nm diameter particle chemical composition by thermal desorption chemical  
783 ionization mass spectrometry, *Aerosol Sci. Technol.*, 38, 100-110,  
784 doi:10.1080/02786820490249036, 2004.

785 Tam, M., and Hill, H. H.: Secondary electrospray ionization-ion mobility spectrometry for  
786 explosive vapor detection, *Anal. Chem.*, 76, 2741-2747, doi:10.1021/ac0354591, 2004.

787 Trostl, J., Chuang, W. K., Gordon, H., Heinritzi, M., Yan, C., Molteni, U., Ahlm, L., Frege, C.,  
788 Bianchi, F., Wagner, R., Simon, M., Lehtipalo, K., Williamson, C., Craven, J. S.,  
789 Duplissy, J., Adamov, A., Almeida, J., Bernhammer, A. K., Breitenlechner, M., Brilke, S.,  
790 Dias, A., Ehrhart, S., Flagan, R. C., Franchin, A., Fuchs, C., Guida, R., Gysel, M., Hansel,  
791 A., Hoyle, C. R., Jokinen, T., Junninen, H., Kangasluoma, J., Keskinen, H., Kim, J.,  
792 Krapf, M., Kurten, A., Laaksonen, A., Lawler, M., Leiminger, M., Mathot, S., Mohler, O.,  
793 Nieminen, T., Onnela, A., Petaja, T., Piel, F. M., Miettinen, P., Rissanen, M. P., Rondo,  
794 L., Sarnela, N., Schobesberger, S., Sengupta, K., Sipila, M., Smith, J. N., Steiner, G.,  
795 Tome, A., Virtanen, A., Wagner, A. C., Weingartner, E., Wimmer, D., Winkler, P. M.,  
796 Ye, P. L., Carslaw, K. S., Curtius, J., Dommen, J., Kirkby, J., Kulmala, M., Riipinen, I.,  
797 Worsnop, D. R., Donahue, N. M., and Baltensperger, U.: The role of low-volatility  
798 organic compounds in initial particle growth in the atmosphere, *Nature*, 533, 527-531,  
799 doi:10.1038/nature18271, 2016.

800 Tu, P. J., Hall, W. A., and Johnston, M. V.: Characterization of Highly Oxidized Molecules in  
801 Fresh and Aged Biogenic Secondary Organic Aerosol, *Anal. Chem.*, 88, 4495-4501, 2016.

802 Veres, P., Roberts, J. M., Warneke, C., Welsh-Bon, D., Zahniser, M., Herndon, S., Fall, R., and  
803 de Gouw, J.: Development of negative-ion proton-transfer chemical-ionization mass  
804 spectrometry (NI-PT-CIMS) for the measurement of gas-phase organic acids in the  
805 atmosphere, *Int. J. Mass Spectrom.*, 274, 48-55, 2008.

806 Whitehouse, C.M., Levin, F., Meng, C.K., Fenn, J.B.: Proceedings of the 34th ASMS  
807 Conference on Mass Spectrometry and Allied Topics, Denver, 507, 1986.

808 Witkowski, B., and Gierczak, T.: Analysis of alpha-acyloxyhydroperoxy aldehydes with  
809 electrospray ionization-tandem mass spectrometry (ESI-MS<sup>n</sup>), *J. Mass Spectrom.*, 48, 79-  
810 88, doi:10.1002/jms.3130, 2013.

811 Wu, C., Siems, W. F., and Hill, H. H.: Secondary electrospray ionization ion mobility  
812 spectrometry/mass spectrometry of illicit drugs, *Anal. Chem.*, 72, 396-403,  
813 doi:10.1021/Ac9907235, 2000.

814 Yatavelli, R. L. N., Lopez-Hilfiker, F., Wargo, J. D., Kimmel, J. R., Cubison, M. J., Bertram, T.  
815 H., Jimenez, J. L., Gonin, M., Worsnop, D. R., and Thornton, J. A.: A Chemical  
816 Ionization High-Resolution Time-of-Flight Mass Spectrometer Coupled to a Micro  
817 Orifice Volatilization Impactor (MOVI-HRToF-CIMS) for Analysis of Gas and Particle-  
818 Phase Organic Species, *Aerosol Sci. Technol.*, 46, 1313-1327,  
819 doi:10.1080/02786826.2012.712236, 2012.

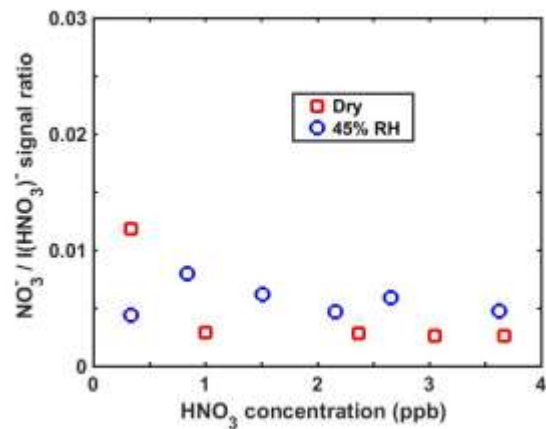
820 Yuan, B., Koss, A., Warneke, C., Gilman, J. B., Lerner, B. M., Stark, H., and de Gouw, J. A.: A  
821 high-resolution time-of-flight chemical ionization mass spectrometer utilizing hydronium  
822 ions (H<sub>3</sub>O<sup>+</sup> ToF-CIMS) for measurements of volatile organic compounds in the  
823 atmosphere, *Atmos. Meas. Tech.*, 9, 2735-2752, doi:10.5194/amt-9-2735-2016, 2016.

824 Zhang, X., Lambe, A. T., Upshur, M. A., Brooks, W. A., Gray Be, A., Thomson, R. J., Geiger, F.  
825 M., Surratt, J. D., Zhang, Z., Gold, A., Graf, S., Cubison, M. J., Groessler, M., Jayne, J. T.,  
826 Worsnop, D. R., and Canagaratna, M. R.: Highly Oxygenated Multifunctional  
827 Compounds in  $\alpha$ -Pinene Secondary Organic Aerosol, *Environ. Sci. Technol.*, 51, 5932-  
828 5940, doi:10.1021/acs.est.6b06588, 2017.

829 Zhao, J., Eisele, F. L., Titcombe, M., Kuang, C. G., and McMurry, P. H.: Chemical ionization  
830 mass spectrometric measurements of atmospheric neutral clusters using the cluster-CIMS,  
831 *J. Geophys. Res.*, 115, 2010.  
832 Zhao, J., Ortega, J., Chen, M., McMurry, P. H., and Smith, J. N.: Dependence of particle  
833 nucleation and growth on high-molecular-weight gas-phase products during ozonolysis of  
834 alpha-pinene, *Atmos. Chem. Phys.*, 13, 7631-7644, 2013.  
835 Zhao, Y., Wingen, L. M., Perraud, V., Greaves, J., and Finlayson-Pitts, B. J.: Role of the reaction  
836 of stabilized Criegee intermediates with peroxy radicals in particle formation and growth  
837 in air, *Phys. Chem. Chem. Phys.*, 17, 12500-12514, doi:10.1039/C5cp01171j, 2015.  
838 Zhao, Y., Wingen, L. M., Perraud, V., and Finlayson-Pitts, B. J.: Phase, composition, and growth  
839 mechanism for secondary organic aerosol from the ozonolysis of  $\alpha$ -cedrene, *Atmos.*  
840 *Chem. Phys.*, 16, 3245-3264, 2016.  
841 Zhu, J. J., Bean, H. D., Kuo, Y. M., and Hill, J. E.: Fast Detection of Volatile Organic  
842 Compounds from Bacterial Cultures by Secondary Electrospray Ionization-Mass  
843 Spectrometry, *J. Clin. Microbiol.*, 48, 4426-4431, doi:10.1128/Jcm.00392-10, 2010.  
844

845





带格式的: 字体颜色: 自动设置

带格式的: 字体颜色: 自动设置

853

854

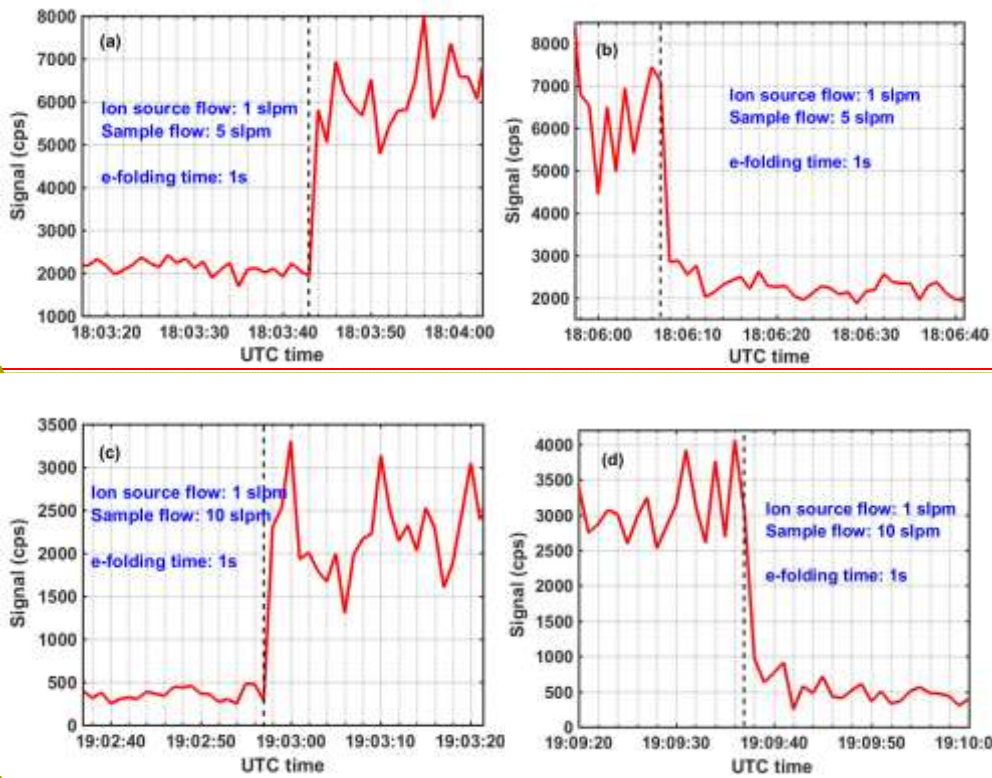
855

856

**Figure 2** Signal ratio of  $\text{NO}_3^- / \text{I}(\text{HNO}_3)^-$  as a function of  $\text{HNO}_3$  concentration under dry and wet conditions observed using iodide as the reagent ion.

带格式的: 字体: 加粗, 字体颜色: 自动设置

带格式的: 字体颜色: 自动设置



带格式的: 字体: (默认) Times New Roman, 12 磅

带格式的: 字体颜色: 自动设置

带格式的: 字体: (默认) Times New Roman, 12 磅

带格式的: 字体颜色: 自动设置

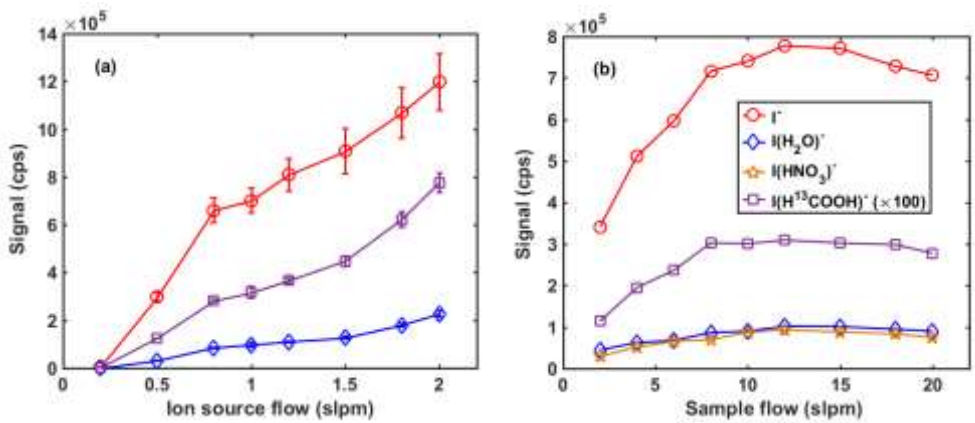
**Figure 3** Time series of  $I(\text{HNO}_3)^-$  observed when sampling (a, b) 5 slpm or (c, d) 10 slpm humid room air containing some ambient  $\text{HNO}_3$  vapor. The ion source flow was 1 slpm. The dashed line indicates the time at which the  $\text{HNO}_3$  standard gas was added or shut off.

带格式的: 字体: 加粗, 字体颜色: 自动设置

带格式的: 字体颜色: 自动设置

带格式的: 字体颜色: 自动设置

带格式的: 字体颜色: 自动设置



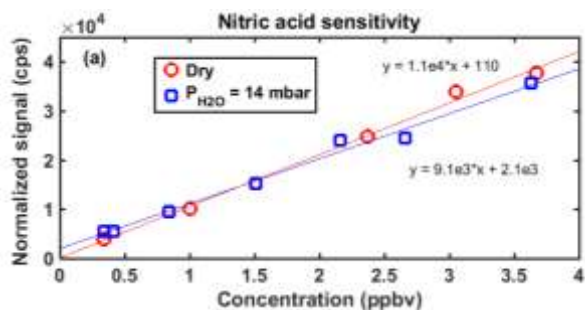
869

870 | **Figure 2-4** Dependence of ion signals on the ion source flow and sample flow. (a) Ion signals  
 871 observed as a function of ion source flow during the sampling of humid room air (15 mbar water  
 872 vapor pressure) containing  $H^{13}COOH$  at a flow of 10 slpm. (b) Ion signals observed during the  
 873 sampling of humid room air containing  $H^{13}COOH$  and  $HNO_3$  at flow rates of 2-20 slpm (the  
 874 ratio of ion source flow/sample flow is fixed to be 1:10). The signals for  $I(H^{13}COOH)^-$  in (a) and  
 875 (b) are magnified by 100 times.

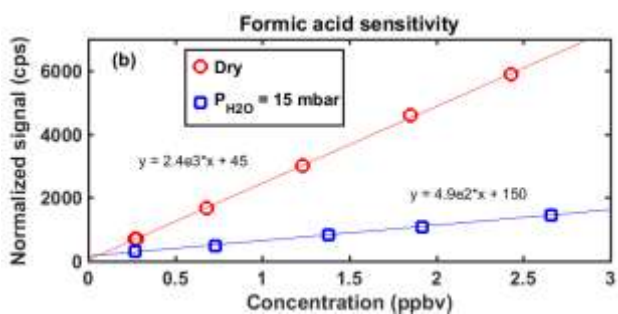
876

877

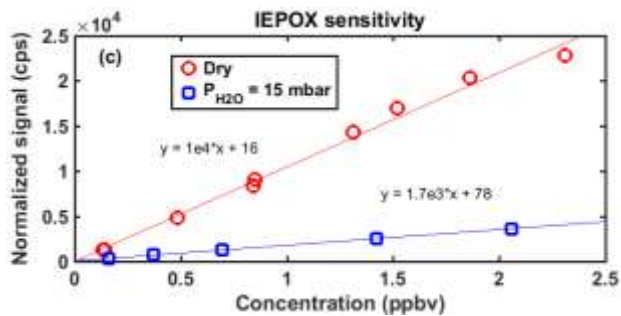
878



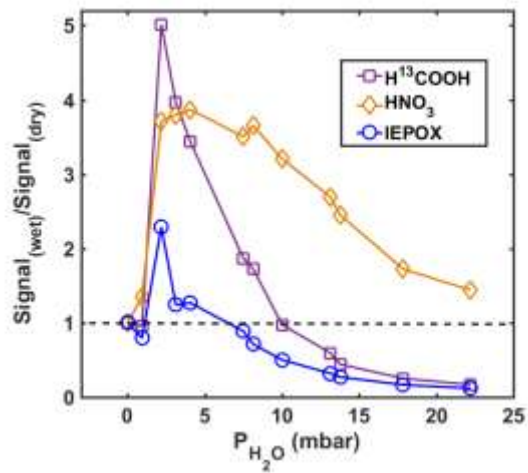
879



880



881 | **Figure 3-5** Normalized The sensitivity to (a) nitric acid, (b) formic acid, and (c) IEPOX under  
882 dry and humid (14 or 15 mbar water vapor pressure) conditions. Signals are normalized by the  
883 ratio of observed total reagent ion count rates to a million ion count rate. The normalized signals  
884 were observed to be a linear function of the delivered concentration. The slope derived from a  
885 linear fit corresponds to the sensitivity per million reagent ion count rates.

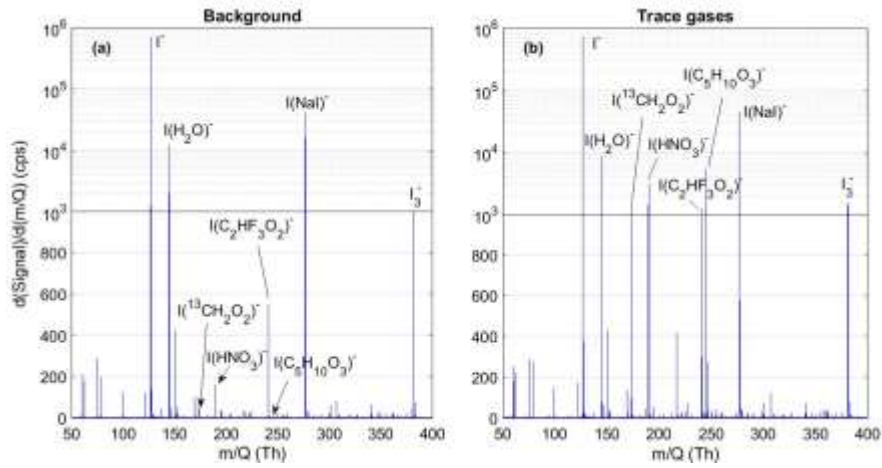


886

887 | **Figure 4.6** Normalized signal of  $I(HNO_3)^-$ ,  $I(H^{13}COOH)^-$ , and  $I(IEPOX)^-$  as a function of water  
 888 vapor pressure ( $P_{H_2O}$ ) in the IMR. The signal of iodide-analyte clusters is first normalized by the  
 889 total reagent ion ( $I^-$  and  $I(H_2O)^-$ ) signals. The resulting normalized signal at each  $P_{H_2O}$  was then  
 890 normalized again to the respective value under dry conditions ( $P_{H_2O} = 0$ , dry UHP  $N_2$ ).

891

892

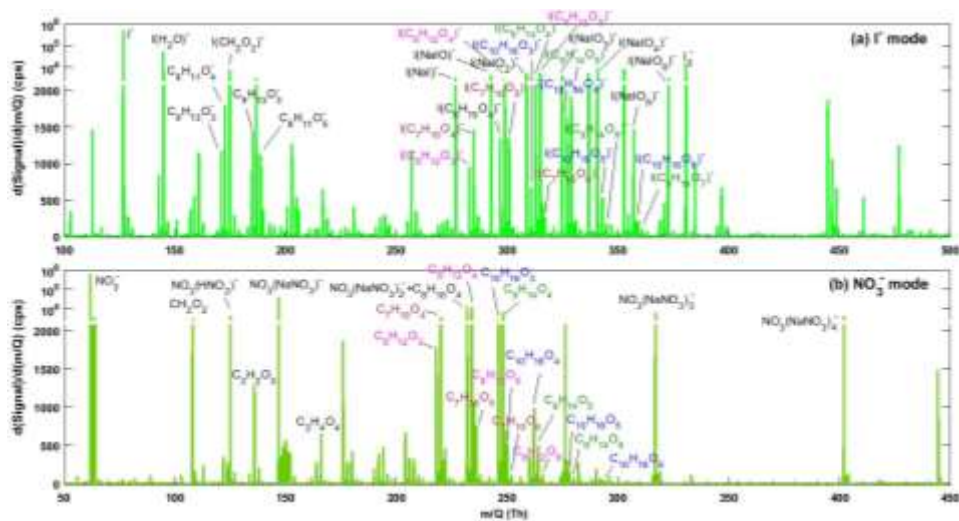


893

894 | **Figure 5-7** High resolution mass spectra collected when sampling (a) UHP N<sub>2</sub> and (b) UHP N<sub>2</sub>  
895 containing HNO<sub>3</sub>, H<sup>13</sup>COOH, and IEPOX gases.

896

897

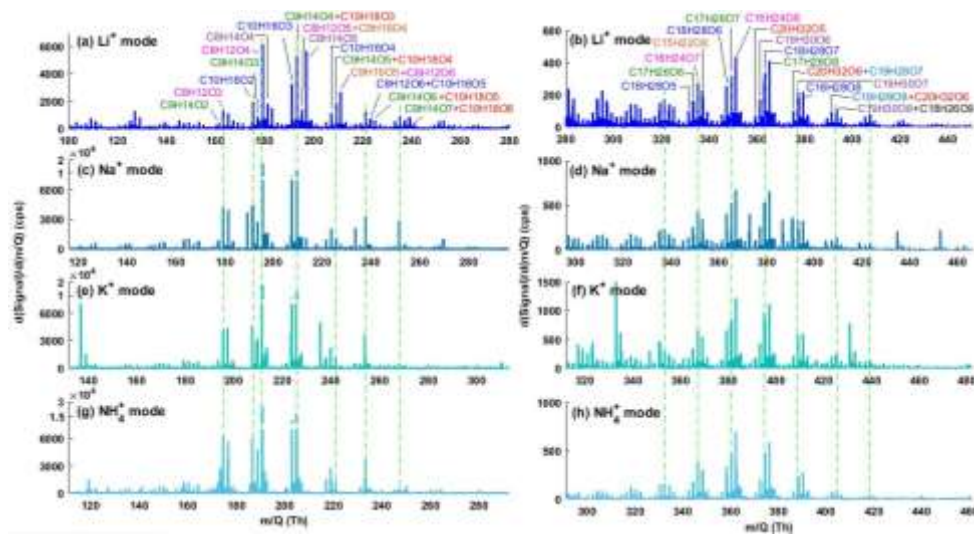


898

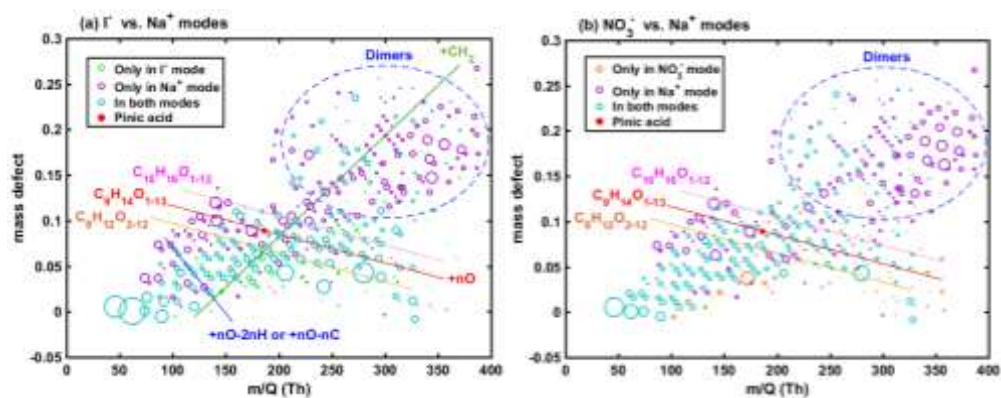
899 **Figure 6.8** High resolution mass spectra obtained during ozonolysis of  $\alpha$ -pinene in a steady-state  
900 chamber using (a) I<sup>-</sup> and (b) NO<sub>3</sub><sup>-</sup> modes. For NO<sub>3</sub><sup>-</sup> mode, the chemical formulae of organic ion  
901 clusters are shown without the corresponding NO<sub>3</sub><sup>-</sup> adduct for clarity as, unlike I<sup>-</sup> mode, organic  
902 ions without a NO<sub>3</sub><sup>-</sup> adduct were negligible components of the spectrum.

903

904



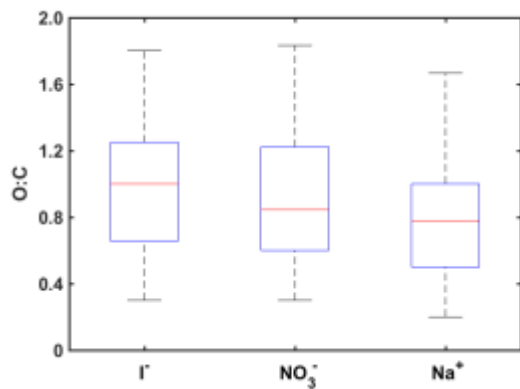
912



913

914 | **Figure 8-10** Comparisons of mass defect plots derived in (a) I<sup>-</sup> and Na<sup>+</sup> modes, and (b) NO<sub>3</sub><sup>-</sup> and  
915 | Na<sup>+</sup> modes during ozonolysis of  $\alpha$ -pinene in a steady-state chamber. To compare the mass defect  
916 | plot obtained in two different ion modes, the reagent ions in observed clusters are excluded for  
917 | the mass defect calculation, and the signals are normalized to the corresponding pinic acid  
918 | intensity in each mode (see text for details). The purple circles do not necessarily mean such ions  
919 | were undetected in the negative mode as they may have very small signal (< 5 cps) and be  
920 | excluded for the high-resolution fitting.

921



922

923

924

925

926

**Figure 11** Boxplots showing the 5th, 25th, 50th, 75th, and 95th percentiles for the O:C ratio of monomeric products from  $\alpha$ -pinene ozonolysis detected in different ion modes.

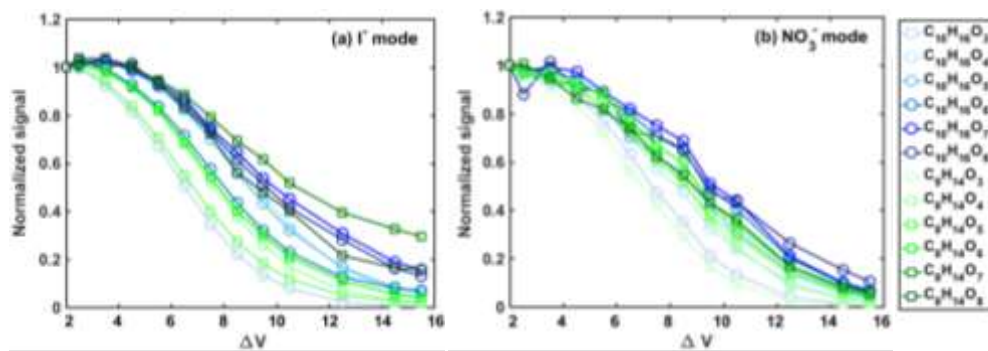
带格式的: 字体: (默认) Times New Roman, 12 磅

带格式的: 字体颜色: 自动设置

带格式的: 字体: 加粗, 字体颜色: 自动设置

带格式的: 字体颜色: 自动设置

927

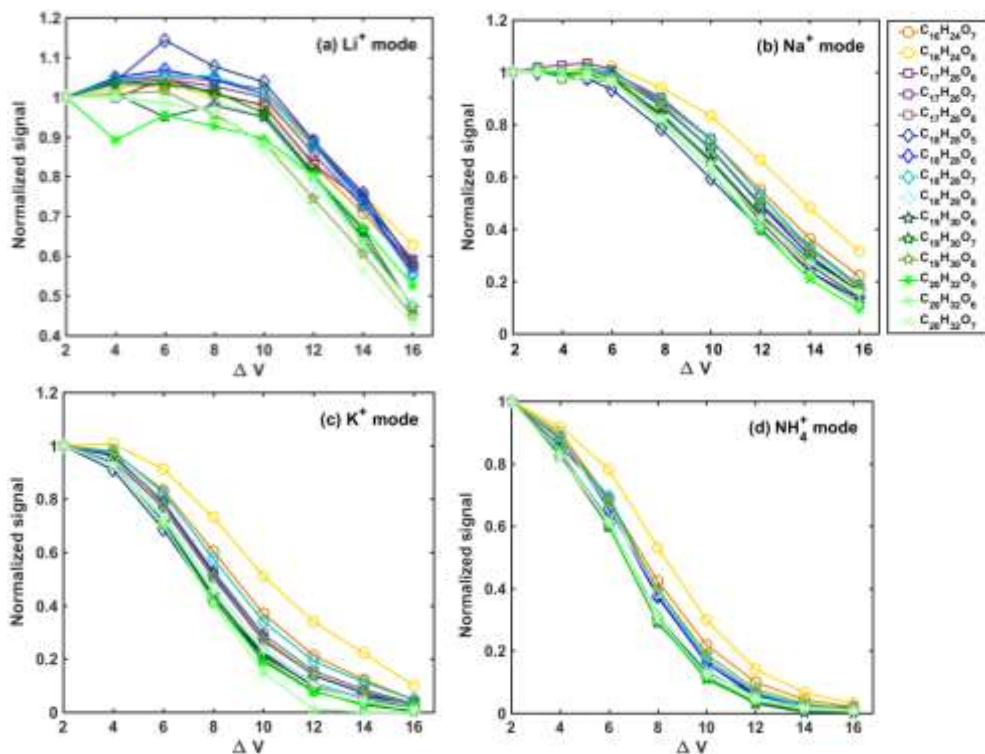


928

929 | **Figure 9-12** Declustering scans of products  $C_{10}H_{16}O_{2-8}$  and  $C_9H_{14}O_{3-8}$  formed by the ozonolysis  
930 of  $\alpha$ -pinene in (a)  $\Gamma$  and (b)  $NO_3^-$  modes.  $\Delta V$  denotes the voltage differences between the end of  
931 first and the entrance to the second quadrupole sections of the mass spectrometer. Signals at  
932 each  $\Delta V$  are normalized to that obtained at the weakest declustering strength (i.e.,  $\Delta V=2$  V).

933

934



935

936

937 | **Figure 10-13** Declustering scans of 15 most abundant dimers formed by the ozonolysis of  $\alpha$ -  
938 pinene in (a)  $Li^+$  mode, (b)  $Na^+$  mode, (c)  $K^+$  mode, and (d)  $NH_4^+$  mode.  $\Delta V$  denotes the voltage  
939 differences between the first and second quadrupole sections of the mass spectrometer. Signals  
940 at each  $\Delta V$  are normalized to that obtained at the weakest declustering strength (i.e.,  $\Delta V = 2$  V).

941